Science Advances
AAAS

advances.sciencemag.org/cgi/content/full/5/11/eaax9171/DC1

Supplementary Materials for

Trace CO_2 capture by an ultramicroporous physisorbent with low water affinity

Soumya Mukherjee, Nivedita Sikdar, Daniel O'Nolan, Douglas M. Franz, Victoria Gascón, Amrit Kumar, Naveen Kumar, Hayley S. Scott, David G. Madden, Paul E. Kruger, Brian Space, Michael J. Zaworotko*

*Corresponding author. Email: xtal@ul.ie

Published 29 November 2019, *Sci. Adv.* **5**, eaax9171 (2019)
DOI: 10.1126/sciadv.aax9171

This PDF file includes:

Supplementary Materials and Methods

Powder X-ray Diffraction (PXRD). Diffractograms were recorded using a PANalytical Empyrean™ diffractometer equipped with a PIXcel^{3D} detector operating in scanning line detector mode with an active length of 4 utilizing 255 channels. The diffractometer is outfitted with an Empyrean Cu LFF (long fine-focus) HR (9430 033 7310x) tube operated at 40 kV and 40 mA and CuK$_\alpha$ radiation (λ_α = 1.540598 Å) was used for diffraction experiments. Continuous scanning mode with the goniometer in the theta-theta orientation was used to collect the data. Incident beam optics included the Fixed Divergences slit with anti-scatter slit PreFIX module, with a 1/8° divergence slit and a 1/4° anti-scatter slit, as well as a 10 mm fixed incident beam mask and a Soller slit (0.04 rad). Divergent beam optics included a P7.5 anti-scatter slit, a Soller slit (0.04 rad), and a Ni-β filter. In a typical experiment, 20 mg of sample was dried, ground into a fine powder and was loaded on a zero background silicon disks. The data was collected from 5°–45° (2θ) with a step-size of 0.0131303° and a scan time of 30 seconds per step. Crude data were analyzed using the X'Pert HighScore Plus™ software V 4.1 (PANalytical, The Netherlands).

Variable Temperature Powder X-ray Diffraction (VT-PXRD). Diffractograms at different temperature were recorded using a PANalytical X'Pert Pro-MPD diffractometer equipped with a PIXcel^{3D} detector operating in scanning line detector mode with an active length of 4 utilizing 255 channels. Anton Paar TTK 450 stage coupled with the Anton Paar TCU 110 Temperature Control Unit was used to record the variable temperature diffractograms. The diffractometer is outfitted with an Empyrean Cu LFF (long fine-focus) HR (9430 033 7300x) tube operated at 40 kV and 40 mA and CuK$_\alpha$ radiation (λ_α = 1.54056 Å) was used for diffraction experiments. Continuous scanning mode with the goniometer in the theta-theta orientation was used to collect the data. Incident beam optics included the Fixed Divergences slit, with a 1/4° divergence slit and a Soller slit (0.04 rad). Divergent beam optics included a

P7.5 anti-scatter slit, a Soller slit (0.04 rad), and a Ni-β filter. In a typical experiment, 20 mg of sample was dried, ground into a fine powder and was loaded on a zero background sample holder made for Anton Paar TTK 450 chamber. The data was collected from 5°–45° (2θ) with a step-size of 0.0167113° and a scan time of 50 seconds per step. Crude data were analyzed using the X'Pert HighScore Plus™ software V 4.1 (PANalytical, The Netherlands).

***In-situ* Powder X-ray Diffraction (*In-situ* PXRD).** *In-situ* diffractograms, 5°–40° (2θ) were recorded using a Cryo & Humidity Chamber: CHC plus$^+$ equipped with a Panalytical Empyrean with Cu tube (40kV and 40mA) in Bragg-Brentano configuration. CHC plus+ is a combination of the multi-purpose CHC Cryo & Humidity Chamber and an advanced humidity (RH) generator for the analysis of humidity-dependent and/or temperature-dependent structural changes in solids using powder X-ray diffraction. Incident side optics: 10 mm beam mask, 0.25° fixed divergence slit. Diffracted side optics: 0.25 fixed anti-scatter slit, Ni filter, Xcelerator detector in 1D mode. In a typical experiment, 20 mg of sample was dried, ground into a fine powder and was loaded on a zero background sample holder made for Anton Paar CHC plus$^+$ chamber. The pressure for the CO_2 experiment was measured along the gas line from the chamber (at 30 °C and 1 bar). For the humidity measurement, 90 % relative humidity (RH) at 30 °C was used. Crude data were analyzed using the X'Pert HighScore Plus™ software V 4.1 (PANalytical, The Netherlands).

Thermogravimetric Analysis (TGA). Thermograms were recorded under nitrogen using TGA instrument TA Q50 V20.13 Build 39. Platinum pans and a flow rate of 60 cm^3 min^{-1} for the nitrogen gas were used for the experiments. The data was collected in the High Resolution Dynamic mode with a sensitivity of 1.0, a resolution of 4.0, and a temperature ramp of 20 °C min^{-1} up to 500 °C. The data was evaluated using the T.A. Universal Analysis suite for Windows XP/Vista Version 4.5A.

Recyclability tests (trace CO_2 mixtures: dry and wet). Gravimetric uptakes were recorded under CO_2/N_2 mixture gases of composition: 1000, 3000, 5000, and 10,000 ppm CO_2 (each,

without and with 74 % RH) saturated with N_2, using TGA instrument TA Q50 V20.13 Build 39. Platinum pans and a flow rate of 20 cm^3 min^{-1} for the mixture gases were used for the experiments. Desorption at 348 K was performed under N_2 flow of 20 cm^3 min^{-1}. The data was collected in the High Resolution Dynamic mode with a sensitivity of 1.0, a resolution of 4.0, and the weight changes during CO_2 adsorption step were monitored under isothermal condition at 303 K. The data was evaluated using the T.A. Universal Analysis suite for Windows XP/Vista Version 4.5A. All the dry and wet mixture gas compositions were set by monitoring Hiden HPR-20 QIC MS.

Particle size distribution (PSD). Number-based particle size distribution (PSD) was measured using Malvern Morphologi G3SE microscopic-image-analysis instrument. A standard operating procedure (SOP) defined to disperse the sample of particles using a sample dispersion unit (SDU-5541 mm^2 area) on a glass plate (180 x 110 mm) with an injection pressure of 4.0 bar, the injection time of 10 minutes and a settling time of 60 seconds. A diascopic light passed from the bottom of the glass plate with automatic light calibration intensity with a set value 80 and intensity tolerance to 0.20. A range of particle size from 0.5 μm−40 μm were analysed using 50X (Nikon TU plan ELWD) magnification optics selection. SOP also determines the image analysis parameters like background separation using an automatic estimated threshold value and watershed segmentation method to separate aggregated particles. Length of the particle, which is the longest projection of two points on the major axis of the particle 2-dimensional area, used to determine particle size distribution. Sauter mean diameter value of D32 used to determine the mean size and distribution width determined with D10, D50, and D90.

FE-SEM Measurements. Scanning electron microscopy (SEM) analysis was performed on a Hitachi SU-70 system operating between 3 and 20 kV. In order to inhibit charging of the samples, they were sputter coated with gold for 45 seconds (20 mA current was applied). The stage height was set to 15 mm.

Vacuum Dynamic Vapour Sorption (DVS) Measurements. Vacuum dynamic vapour sorption (DVS) measurements were conducted using a Surface Measurement System DVS Vacuum device (London, UK). The DVS instrument used for these studies measures the uptake and loss of vapour gravimetrically. DVS methods were used for the determination of water vapour sorption isotherms. The experiments were performed in a temperature-controlled incubator at different temperatures (298 K, 303 K, 308 K and 323 K). Activated and degassed samples were further degassed *in-situ* under high vacuum ($2 \cdot 10^{-6}$ Torr) to stablish the dry mass. Stepped increases in relative humidity were controlled by equilibrated weight changes of the sample (dm/dt = 0.006 % min^{-1}) from 0 to 95 % RH (P/P_0) in 2 %, 5 % or 10 % incremental RH steps. The P/P_0 was then decreased in a similar manner to accomplish a full adsorption/desorption cycle. Vacuum pressure transducers were used with the ability to measure from $1 \cdot 10^{-6}$ Torr up to 760 Torr with a resolution of 0.01 %. Therefore, the vacuum system with its pre-heater (up to 673 K) allows a complete material degasification. Approximately 20–30 mg of sample were used for each experiment. The mass of every sample was determined by comparison with an empty reference pan and recorded by a high resolution microbalance with a mass resolution of ± 0.1 μg. The high mass resolution and its excellent baseline stability allow the instrument to measure the adsorption and desorption of very small amounts of water molecules. The vapour partial pressure around the sample is controlled by mixing saturated and dry carrier vapour streams using electronic mass flow controllers. The temperature is maintained constant at ± 0.1 K, by enclosing the entire system in a temperature-controlled incubator. Pure water (HPLC Gradient Grade, CAS No. 7732-18-5, Fisher Chemical) was used as the adsorbate for the studies.

Intrinsic Dynamic vapour sorption (DVS) Measurements. Water vapour adsorption–desorption experiments at atmospheric pressure were performed using a dynamic vapour sorption (DVS) intrinsic analyser (from Surface Measurement Systems, London, UK). The DVS Intrinsic is designed to accurately measure sample's mass change as it sorbs high-

precisely controlled concentrations of water vapour using air as a carrier gas. The sample (*ca.* 20–30 mg) was loaded into a stainless steel pan and suspended from an ultra-sensitive recording microbalance (with a resolution of 0.1 μg) with the help of a hang-down wire. Before the experiment started, once the sample was loaded from said hang-down wire, it was allowed to reach temperature and humidity equilibria within its chamber for a short period of time. The sample was exposed to an air flow with known % RH (from 0 % RH to 90 % RH) with increasing/decreasing steps of 10 % RH in the adsorption/desorption branches, respectively. The flow-rate used in the experiments was 200 sccm (Standard Cubic Centimetres per Minute), and the temperatures employed were 298, 300, 303, 308 and 313 K (± 0.2 K to each). Equilibria determination of the sample mass at each RH stage was performed by measuring the change rate percentage of mass over time (dm/dt). Not until said (dm/dt) reached a value of 0.002 % min^{-1}, the equilibria was considered to be achieved (with an accuracy of ± 1.0 % RH), and the device was allowed to measure the next stage of RH. Accordingly, the sample mass readings obtained from the microbalance within said equilibria revealed the vapour adsorption/desorption behaviour of the sample. Consequently, isotherm analysis and kinetics profiles of water vapour sorption and desorption were recorded.

Accelerated Stability Protocol. In a typical experiment, as followed by the pharmaceutical industries (*33, 41*), microcrystalline samples of **SIFSIX-18-Ni-β** were exposed to 313 K and 75 % RH for 1, 7 and 14 days (d) in a desiccator (corresponding to 4 d, 1 month and 2 months shelf-life, respectively). These conditions were achieved by using a supersaturated aqueous solution of NaCl maintained at 313 K in a closed desiccator. After 1, 7 and 14 d, sample aliquots were removed from desiccator and characterized by PXRD and N_2 (77 K) surface area measurements in order to detect signs in the sample which may have been affected by humidity. 298 K CO_2 sorption isotherms were also measured after duly activating each of the humidity exposed samples of **SIFSIX-18-Ni-β**.

Fourier-transform infrared (FT-IR) spectroscopy experiments. FT-IR spectra were obtained on a PerkinElmer Spectrum 100 FT-IR Spectrometer with a resolution setting of 2 and 16 scans per sample. Data was plotted as percent transmittance in Y-axis and analysed using the Spectrum V 6.3 software package.

Supplementary Text

Molar Selectivity (or Ideal Selectivity).

For a binary mixture, the ***adsorption selectivity*** **(S_{ads}** or α_{ij}**)** is defined as follows

$$S_{ads} = \frac{q_i/q_j}{p_i/p_j}$$

$q_{i,j}$ and $p_{i,j}$ denote the uptakes and partial pressures for components *i* and *j*, respectively. This is also referred to as ***Ideal selectivity (IS)*** or ***molar selectivity***.

For 10,000 ppm CO_2/99 % O_2 mixture, q_{CO2} = 2.1 mmol g^{-1}, q_{O2} = 0.1 mmol g^{-1}, p_{CO2} = 0.01, p_{O2} = 0.99, the CO_2/O_2 adsorption selectivity (S_{CO}) is 2,079.

Ideal Adsorbed Solution Theory (IAST).

IAST calculations were carried out using a modified version of the program pyIAST (*29*). We note that the IAST calculations are limited by three assumptions:

(a) The pure components form an ideal mixture (*i.e.* no change in area or enthalpy upon mixing of pure components);

(b) The area accessible to both adsorbates are equal (*i.e.* the sorbent is not a molecular sieve);

(c) The thermodynamic properties of the sorbent do not change relative to the thermodynamic properties of the sorbate (*i.e.* there is no sorbate-induced phase transition).

Isotherm Fitting. The data points of the experimental 298 K isotherms for CO_2, N_2, C_2H_2, and H_2O were interpolated *via* numerical quadrature

$$\frac{A}{RT}\pi_i(P_i^\circ) = \int_0^{P_1} \frac{n_i^\circ(P)}{P} dP + \sum_{j=1}^{k-1} \int_{P_j}^{P_{j+1}} \frac{n_i^\circ(P)}{P} dP + \int_{P_k}^{P_i^\circ} \frac{n_i^\circ(P)}{P} dP \qquad \text{Equation (1)}$$

A model of each isotherm was formulated where the spreading pressure, $\frac{A}{RT}\pi_i(P_i^\circ)$, from absolute vacuum to the first data point is assumed to follow Henry's law

$$n_i^\circ(P) = K_H P \qquad \text{Equation (2)}$$

Where n_i° is uptake, and P is pressure, and therefore

$$\int_0^{P_1} \frac{n_i^\circ(P)}{P} dP \approx \int_0^{P_1} K_H dP = n_i^\circ(P_1) \qquad \text{Equation (3)}$$

Between the first to the last experimental data points, the function $n_i^\circ(P)$ is approximated via linear interpolation where

$$\int_{P_j}^{P_{j+1}} \frac{n_i^\circ(P)}{P} dP \approx m_j\left(P_{j+1} - P_j\right) + b_j \log\left(\frac{P_{j+1}}{P_j}\right) \qquad \text{Equation (4)}$$

m_j is the slope and $b_j$is the intercept of the line that passes through the points $\left(P_j, n_i^\circ\left(P_j\right)\right)$ and $\left(P_{j+1}, n_i^\circ\left(P_{j+1}\right)\right)$. The index k defines the range $P_k \leq P_i^\circ \leq P_{k+1}$. Therefore the integral $\int_{P_k}^{P_i^\circ} \frac{n_i^\circ(P)}{P} dP$ acts in the same way as Eq. 4 but accounting for the line that passes through interpolated points.

Discussion on IAST.

As observable from comparison of the room temperature pure gas isotherms in **SIFSIX-18-Ni-*β***, there is negligible adsorption of N_2 (fig. S10). Such results violate the second

assumption required for IAST calculations. Attempts at IAST calculations resulted in S_{CN} selectivity of > $1x10^7$ and increased with pressure, which suggest that this is indeed the result of partial sieving effects (*partial* since 6.27 mmol g^{-1} N_2). Similar IAST sieving results were obtained for CO_2/O_2 selectivity *i.e.* S_{CO} under varying trace compositions (fig. S46).

Calculations of S_{CW} were carried out on **SIFSIX-18-Ni-β** at CO_2 concentration of 500 ppm, 5000 ppm, and 10,000 ppm at 10–95 % RH. Given the hydrophobic nature of the pore, IAST calculations were calculated based on dynamic vapour sorption experiments conducted under vacuum (where uptake is considered as all water vapour adsorbed into the pore and onto the surface of the particles), minus dynamic vapour sorption experiments conducted under ambient pressure (where uptake is considered as only water vapour adsorbed onto the surface of the particles). IAST calculations for S_{CW} at 74 % RH are shown in table S1. Given the significantly higher uptake of water vapour in **Zeolite 13X** and **Mg-MOF-74**, and the observed negative adsorption in **TIFSIX-3-Ni** and **SIFSIX-3-Ni**, S_{CW} was not calculated for these compounds.

Structural solution of SIFSIX-18-Ni.

Structure solution and refinement of **SIFSIX-18-Ni-α** was carried out in GSAS-II (fig. S55 and table S5) using an overnight scan using the PANalytical Empyrean in reflection mode. The lattice parameters were determined and structure factors obtained *via* the Le Bail method. A Monte Carlo/simulated annealing method was used for structure solution using free moving rigid bodies obtained from the Cambridge Structural Database (CSD) (CSD Refcodes: FUDQIF = SiF_6^{2-}; KIKDOZ = 3,3',5,5'-tetramethyl-1H,1'H-4,4'-bipyrazole).

Structure solution and refinement of **SIFSIX-18-Ni-β** was carried out in GSAS-II and HighScore Plus^{TM} (fig. S56 and table S5) using data collected at 393 K after 1 hour of annealing. The lattice parameters were determined and structure factors obtained via the Pawley method. The inorganic axis was identified from Fourier maps using the charge

flipping method. A Monte Carlo/simulated annealing method was used for further structure solution using free moving rigid bodies obtained from the Cambridge Structural Database (CSD) (CSD Refcodes: FUDQIF = SiF_6^{2-}; WEWHEN = 3,3',5,5'-tetramethyl-1H,1'H-4,4'-bipyrazole). A final Rietveld refinement was carried out in HighScore Plus™ (table S5).

Isosteric Heats of Adsorption Calculations.

The Q_{st} of CO_2 for **SIFSIX-18-Ni-β** was calculated from the low pressure CO_2 adsorption isotherms collected at 273, 283 and 298 K while that for **ZIF-8** was calculated from isotherms recorded at 273 and 293 K. All other Q_{st} plots and associated parameters are included in our earlier contribution (*26*).

The Clausius-Clapeyron equation was used for the calculation of Q_{st} where virial-type equations were used to fit ten points in the adsorption data between 0 and 10,000 ppm at multiple temperatures (Equation (5) below). All fitting was performed using Origin Pro 8

$$\ln P = \ln N + \sum_{i=0}^{m} a_i N_i + \sum_{i=0}^{n} \binom{n}{k} b_i N_i \qquad \text{Equation (5)}$$

Q_{st} was then calculated from the virial model using Equation (6)

$$-Q_{st} = -R \sum_{i=0}^{m} a_i N_i \qquad \text{Equation (6)}$$

Ten adsorption points between 0 and 10,000 ppm (10 mbar) were used for fitting to the Virial equation where the fit for each of the compounds is shown in figs. S19, S20.

Synthesis of materials.

Zeolite 13X was obtained from Sigma-Aldrich. **SIFSIX-3-Ni**, **Mg-MOF-74**, **TIFSIX-3-Ni, ZIF-8** and **NbOFFIVE-1-Ni** were synthesised according to literature procedures (*23*, *25*).

3,3',5,5'-tetramethyl-1H,1'H-4,4'-bipyrazole (18) synthesis.

3,3',5,5'-tetramethyl-1H,1'H-4,4'-bipyrazole (**18**) was synthesized following reported procedure (*42*).

Preparation of [Ni(3,3',5,5'-tetramethyl-1H,1'H-4,4'-bipyrazole)$_2$(SiF_6)]$_n$ (SIFSIX-18-Ni). **SIFISIX-18-Ni** was synthesized by hydrothermal treatment of 3 mmol of $NiSiF_6.xH_2O$ (930 mg), and 6 mmol of ligand **18** (Me_4bpz = 3,3′,5,5′-tetramethyl-4,4′-bipyrazole) in 5 mL of water over 72 hours. The resulting suspension was filtered under vacuum and dried in air to obtain the as-synthesized precursor. This precursor was washed thrice, each with *ca.* 20 mL portion of methanol on a Büchner filter. After air drying, the solid was heated at 55 °C for 24 hours to obtain **SIFSIX-18-Ni-*α***. Activation of **SIFSIX-18-Ni** was achieved by degassing the methanol-exchanged sample on a SmartVacPrep™ using dynamic vacuum and heating for 4 hours (sample heated from RT to 348 K with a ramp rate of 5 K).

Heating **SIFSIX-18-Ni-*α*** under vacuum to 348 K induced a phase transition to **SIFSIX-18-Ni-*β***, which exhibited a 13.4 % reduction in unit cell volume. All properties reported herein were conducted on this activated form of **SIFSIX-18-Ni-*β***. Slow diffusion through MeOH/DCM layers yielded polycrystalline **SIFSIX-18-Ni-*γ***, which was non-porous and isostructural to a previously reported structure (CSD Refcode: KIKDUF). Expectedly, **SIFSIX-18-Ni** forms a primitive cubic, **pcu**, net wherein two-dimensional (2D) nets of metal nodes cross-linked by organic linkers are pillared by inorganic anions, affording square channels lined with inorganic fluorides, organic amines and organic methyl groups. See fig. S12 for 298 K CO_2 gas sorption isotherms for each phase of **SIFSIX-18-Ni**.

Molecular modelling to locate the CO_2 binding sites in SIFSIX-18-Ni.

To determine the optimal binding site of CO_2 in **SIFSIX-18-Ni**, a screening of periodic plane-wave Density Functional Theory calculations were first performed using CP2K (*43*), where a single CO_2 molecule was placed in the cavity of a 1x1x1 cell of **SIFSIX-18-Ni-*α*** and **SIFSIX-18-Ni-*β***. The revPBE XC functional was used with MOLOPT basis sets for all atoms with the DFTD3 pair potential for dispersion correction. These calculations were performed using Unrestricted Kohn-Sham DFT with a total multiplicity of 5 (corresponding to the triplet

spin state for Ni atoms). The sample locations for the sorbate CO_2 were collinear with the F–F line in the cavity (between SIFSIX groups). The distance of the CO_2 molecule's center-of-mass to the nearest F atom ranged from 2-5 Å, and different orientations were sampled by rotating the CO_2 about the C_{CO2}–F axis. A total of 224 unique configurations of CO_2 were sampled, ignoring obvious atomic overlaps. The configuration with lowest CO_2–HUM interaction energy (as calculated by $E_{HUM+CO2} - E_{HUM} - E_{CO2}$) was then treated in a full-atom optimization of the [HUM + CO_2] system using the same methods in CP2K with the Conjugate Gradient algorithm for minimizing the energy of the system. After convergence this resulted in the structure shown in Figure 2f.

For empirical modelling, Canonical Monte Carlo simulations were performed in a 2x2x2 box of **SIFSIX-18-Ni-*β*** using Monte Carlo Molecular Dynamics (MCMD), an open-source code developed by the Space group and available on GitHub (D. M. Franz, *Monte Carlo - Molecular Dynamics, https://github.com/khavernathy/mcmd.* (2017)). The system was filled with CO_2 molecules corresponding to the experimental loading at 298 K and 1 atm and the energy of the system was allowed to relax by random translations and rotations of the CO_2 molecules with acceptance of the moves guided by the Boltzmann factor corresponding to the energy change from the trial move. The UFF forcefield (*44*) was used for all atoms in the HUM, with the Lennard-Jones potential describing repulsion-dispersion interactions between all pairs of atoms. The CO_2-PHAST model (*45*) was used for CO_2 repulsion-dispersion and partial charges. The electrostatics of the system were computed using Ewald summation, and partial charges on the HUM atoms were determined by a RESP fit to the electrostatic surface potential computed using CP2K with the previously described methods. A total of $1x10^7$ Monte Carlo trial moves were conducted to determine the equilibrated structure, after an initial equilibration run with $1x10^6$ steps.

Powder X-ray Diffraction for SIFSIX-18-Ni.

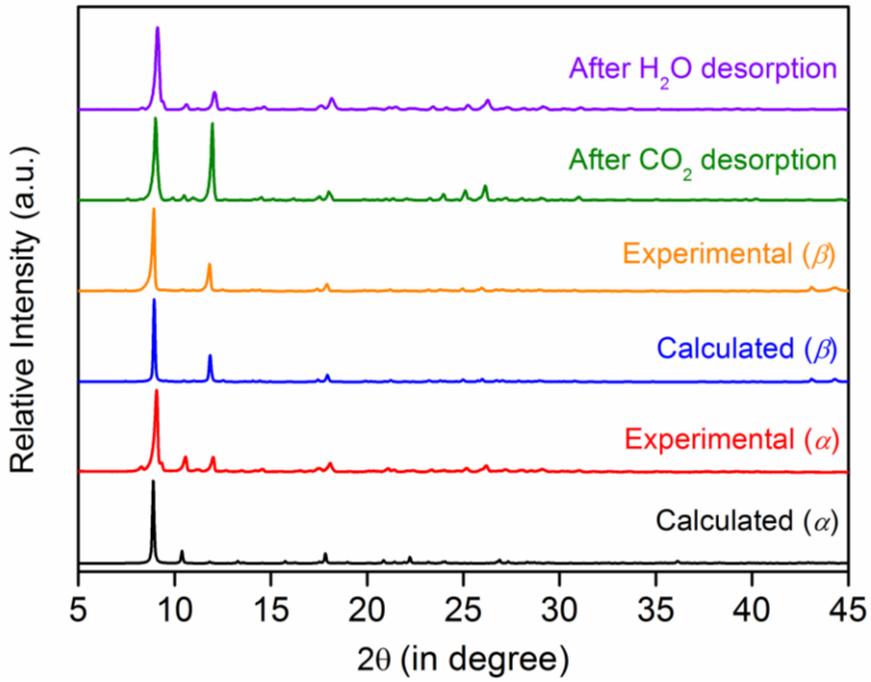

Fig. S1. PXRD of SIFSIX-18-Ni.

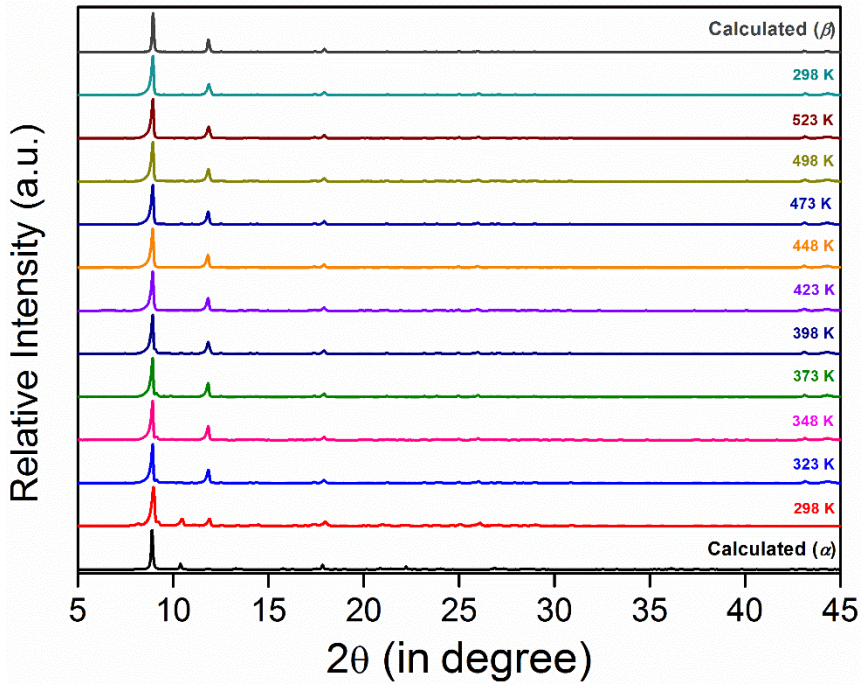

Fig. S2. Variable temperature PXRD of SIFSIX-18-Ni.

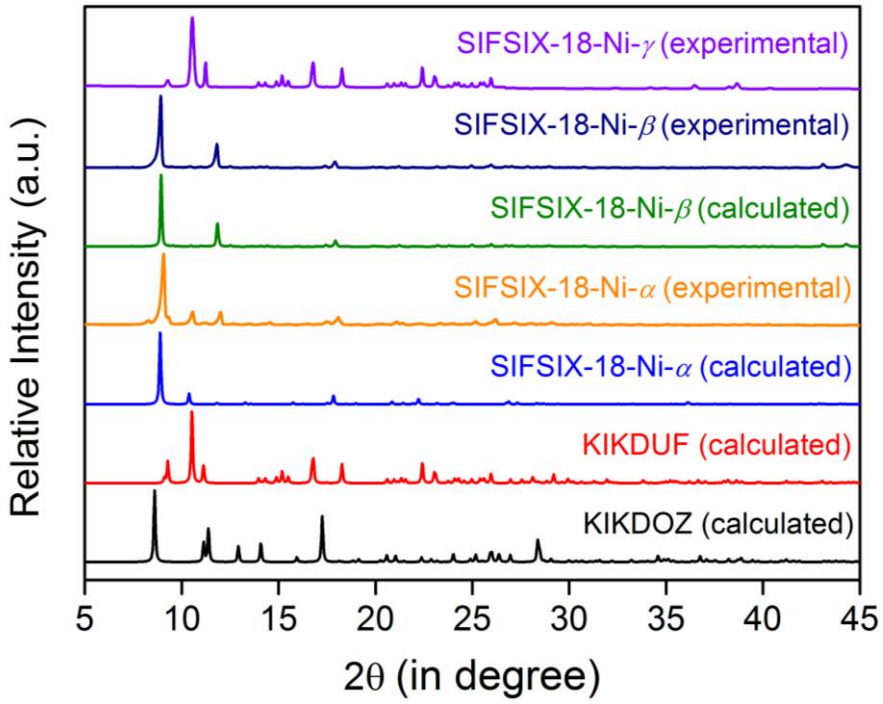

Fig. S3. Comparison of experimental PXRD profiles for SIFSIX-18-Ni-α, SIFSIX-18-Ni-β, and SIFSIX-18-Ni-γ with their calculated patterns and related polymorphs (*24*) (all recorded at 298 K).

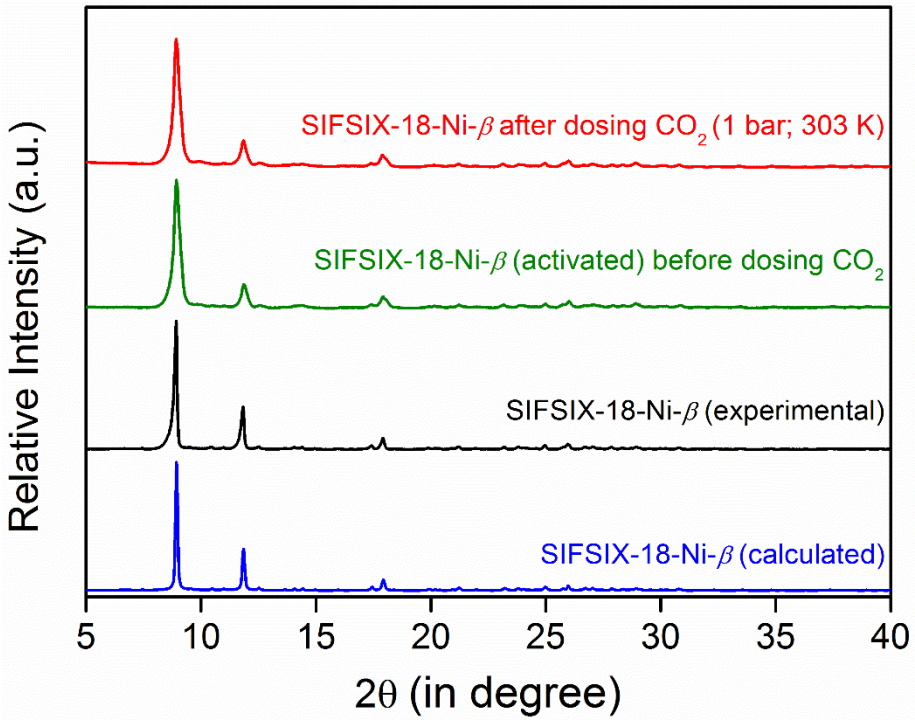

Fig. S4. Comparison of experimental PXRD profiles for SIFSIX-18-Ni-β, SIFSIX-18-Ni-β activated, before dosing CO_2) and SIFSIX-18-Ni-β (dosed with 1 bar CO_2 at 303 K) with the calculated pattern of SIFSIX-18-Ni-β.

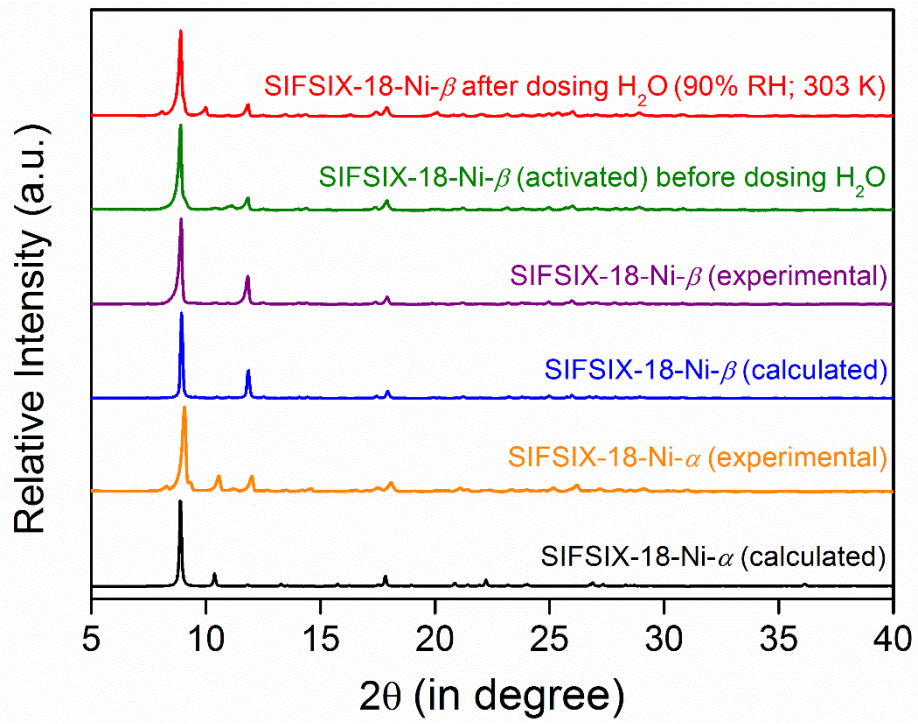

Fig. S5. Comparison of experimental PXRD profiles for SIFSIX-18-Ni-α, SIFSIX-18-Ni-β, and SIFSIX-18-Ni-β activated, before dosing H_2O), and SIFSIX-18-Ni-β (dosed with H_2O vapour under 90 % RH at 303 K) with the calculated patterns of SIFSIX-18-Ni-α and SIFSIX-18-Ni-β.

Particle size distribution for SIFSIX-18-Ni-β.

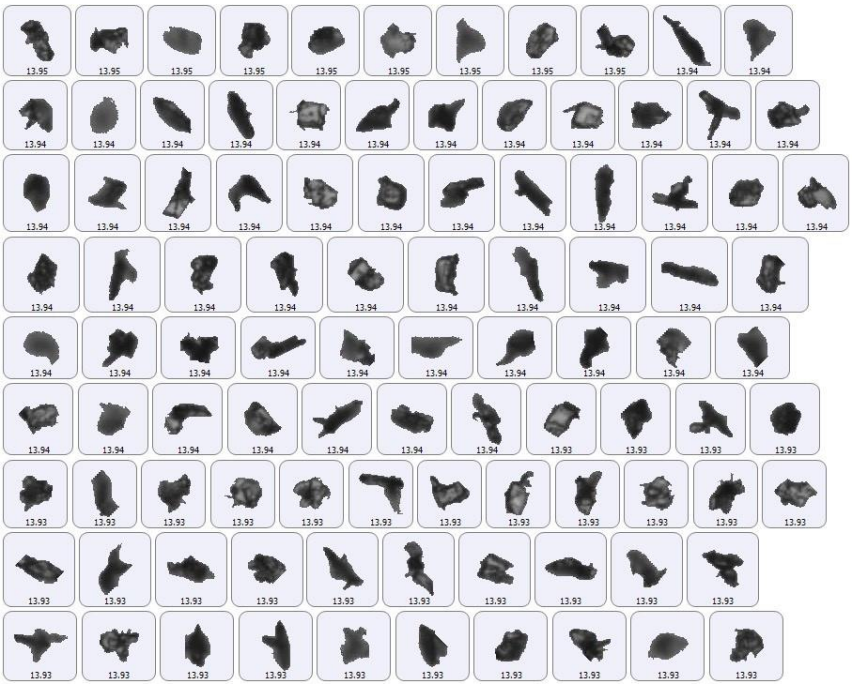

Fig. S6. Particle size distribution around the mean diameter (~13.94 µm) range of SIFSIX-18-Ni-β.

Thermogravimetric Analysis (TGA) for SIFSIX-18-Ni.

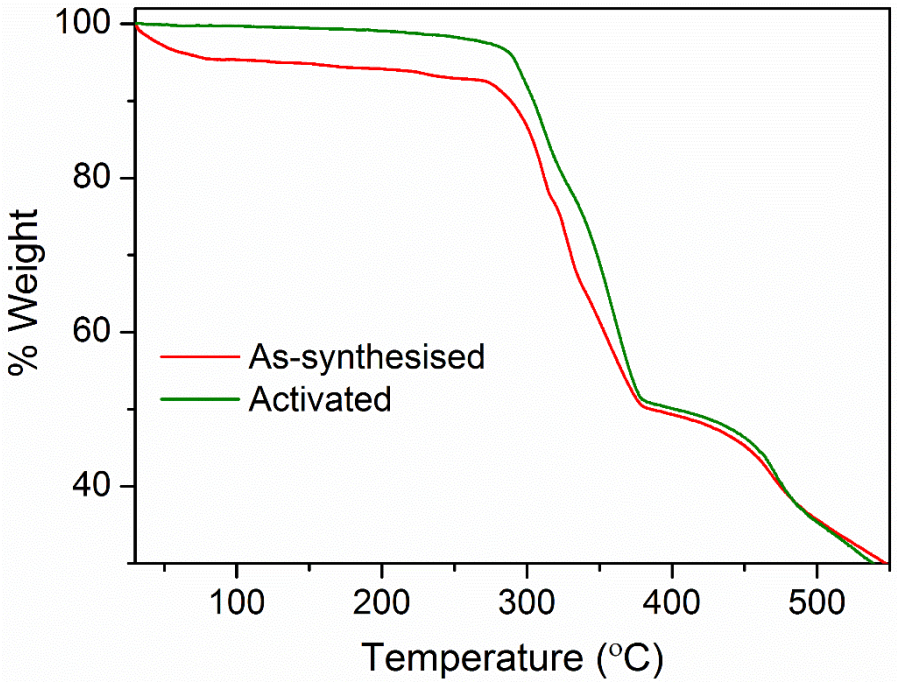

Fig. S7. Thermogravimetric analysis profiles of SIFSIX-18-Ni.

Gas Sorption Isotherms.

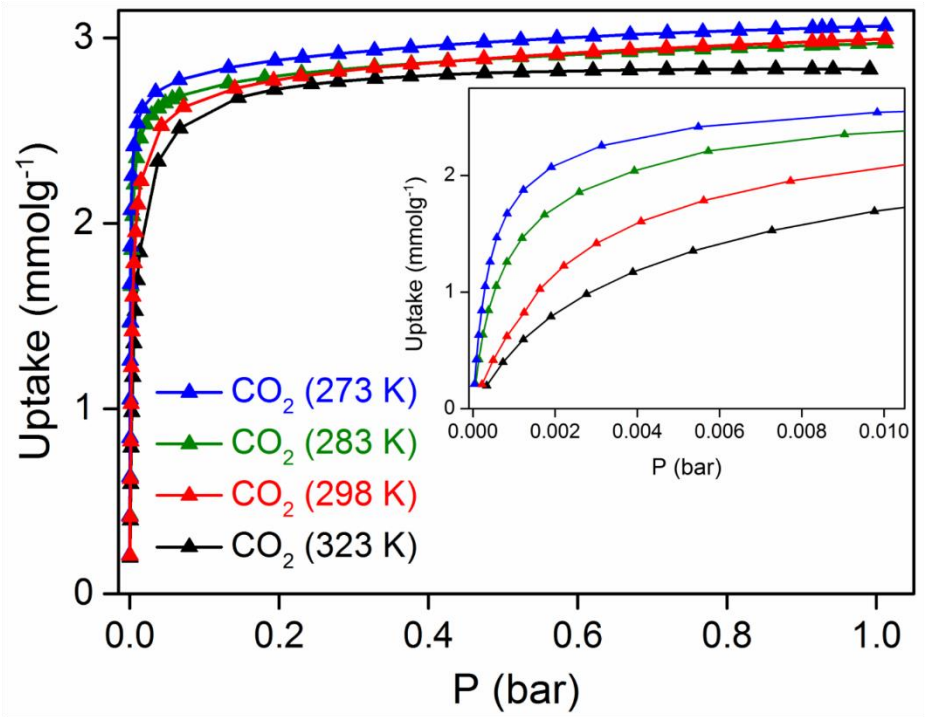

Fig. S8. CO_2 sorption isotherms for SIFSIX-18-Ni-β; inset: low pressure range until 0.01 bar**.**

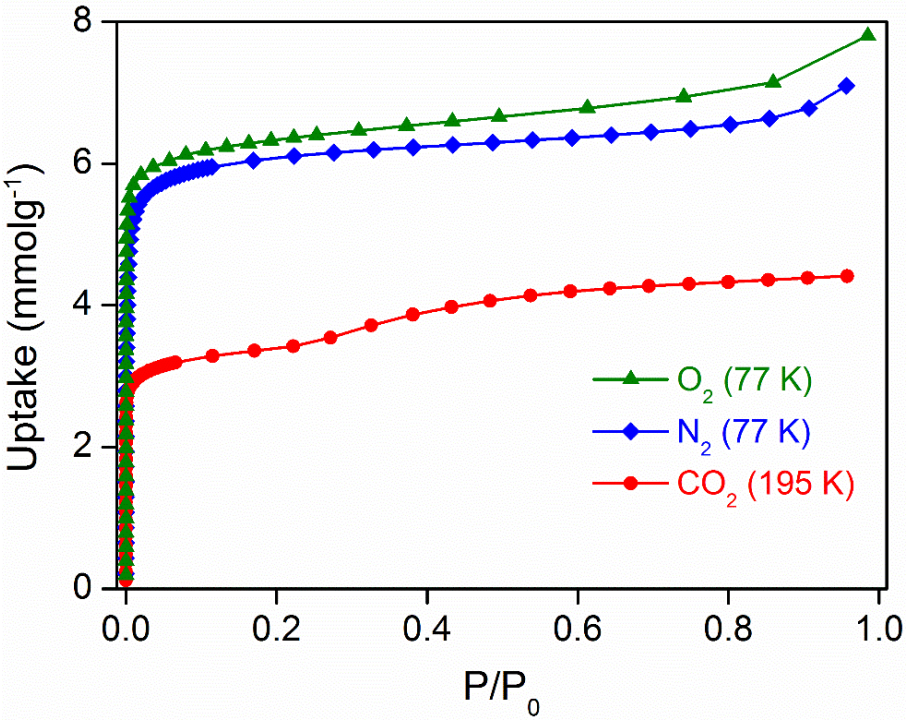

Fig. S9. Low-temperature CO_2, N_2, and O_2 sorption isotherms for SIFSIX-18-Ni-β.

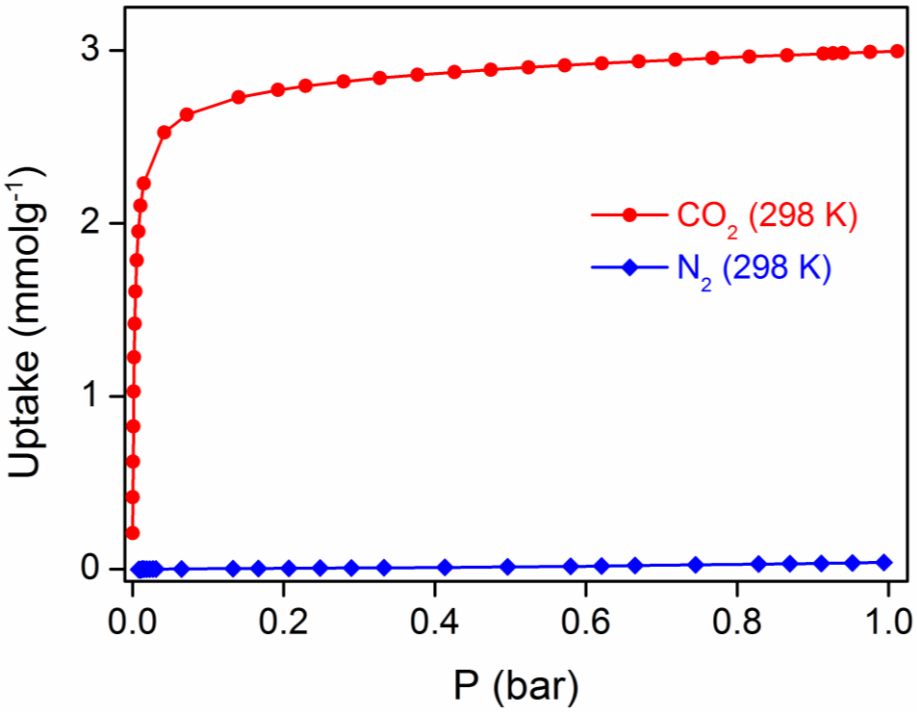

Fig. S10. CO_2 and N_2 sorption isotherms for SIFSIX-18-Ni-β.

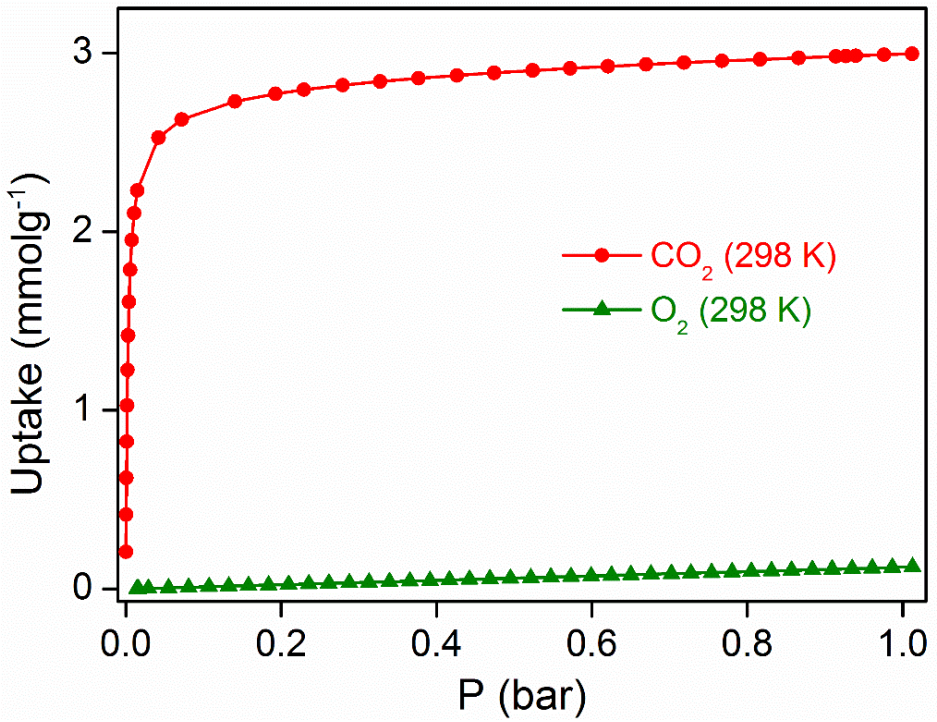

Fig. S11. CO_2 and O_2 sorption isotherms for SIFSIX-18-Ni-β.

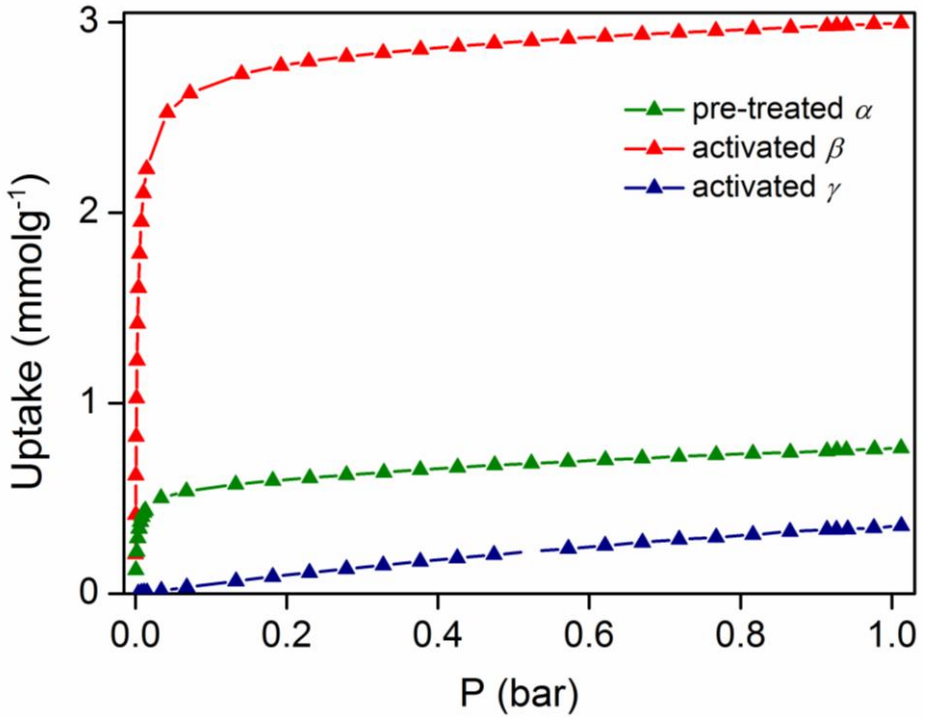

Fig. S12. CO_2 sorption isotherms at 298 K for SIFSIX-18-Ni-α (only subjected to evacuation after MeOH washing of precursor, i.e., no heating), SIFSIX-18-Ni-β and SIFSIX-18-Ni-γ.

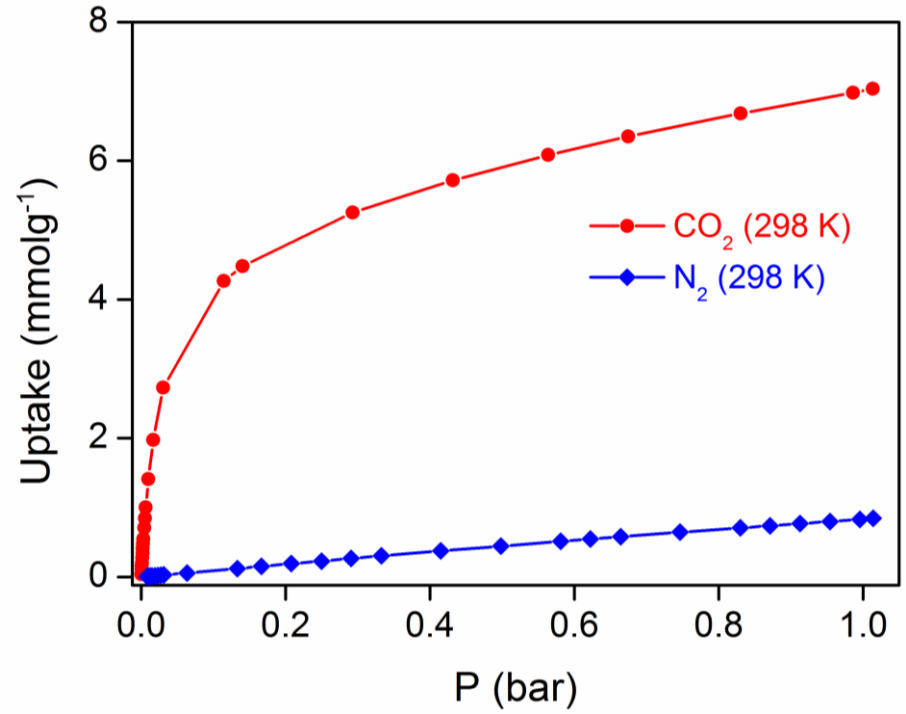

Fig. S13. CO_2 and N_2 sorption isotherms for Mg-MOF-74.

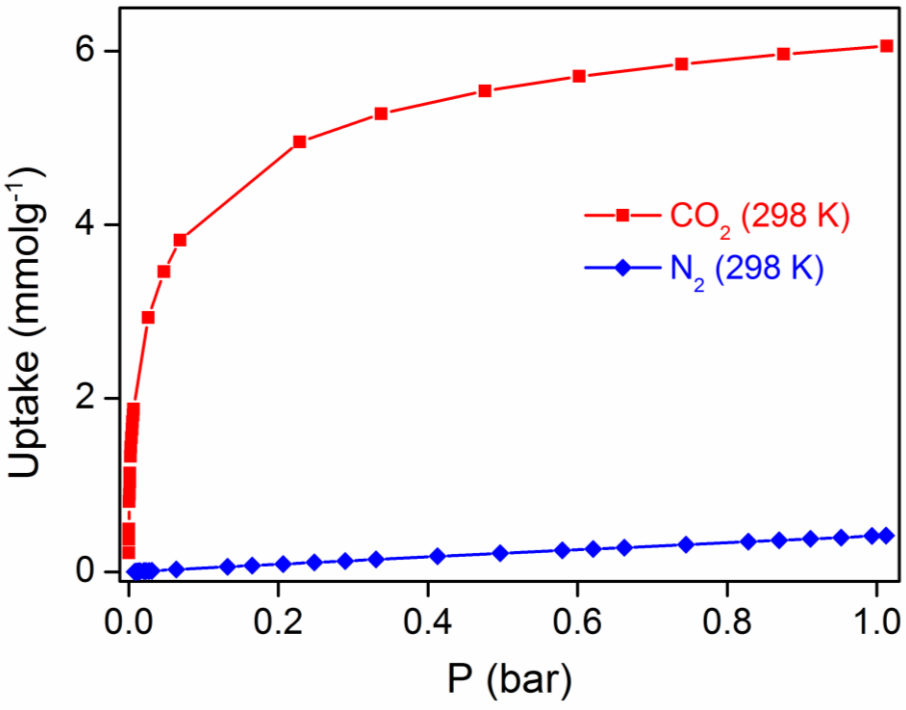

Fig. S14. CO_2 and N_2 sorption isotherms for Zeolite 13X.

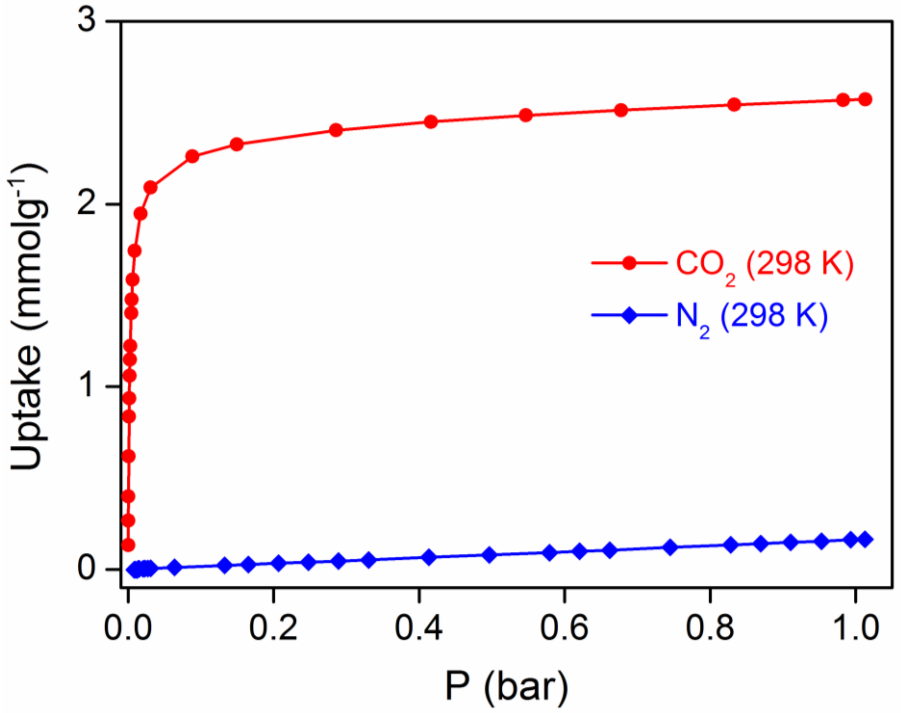

Fig. S15. CO_2 and N_2 sorption isotherms for SIFSIX-3-Ni.

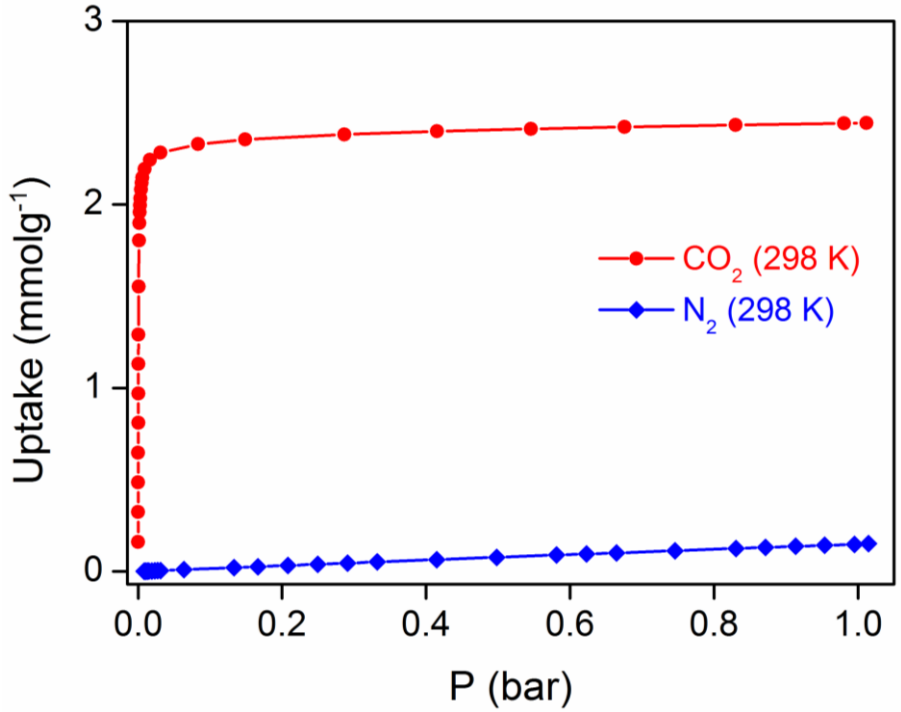

Fig. S16. CO_2 and N_2 sorption isotherms for NbOFFIVE-1-Ni.

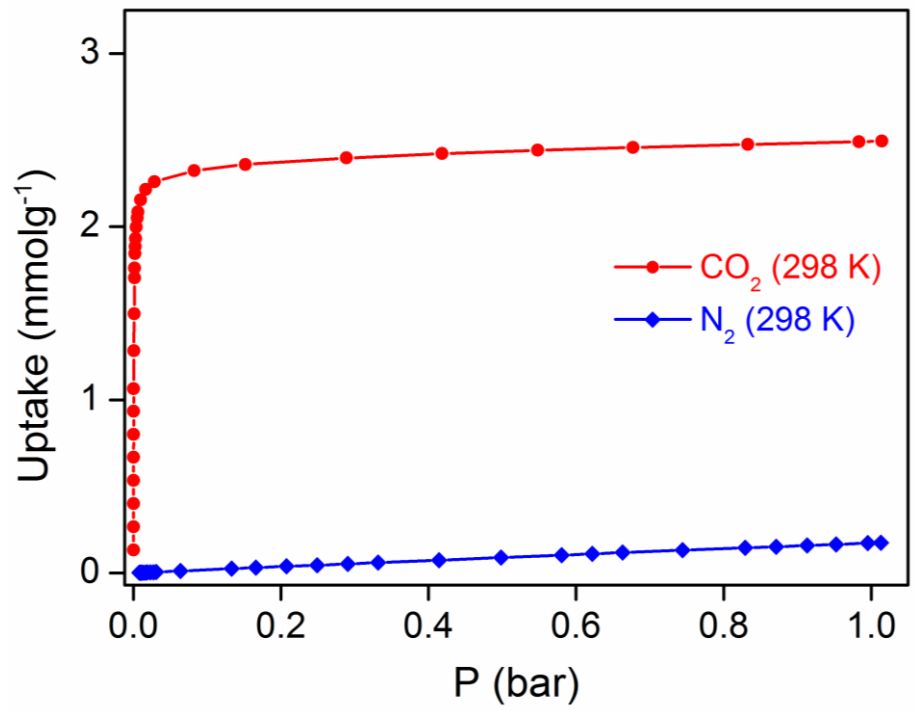

Fig. S17. CO_2 and N_2 sorption isotherms for TIFSIX-3-Ni.

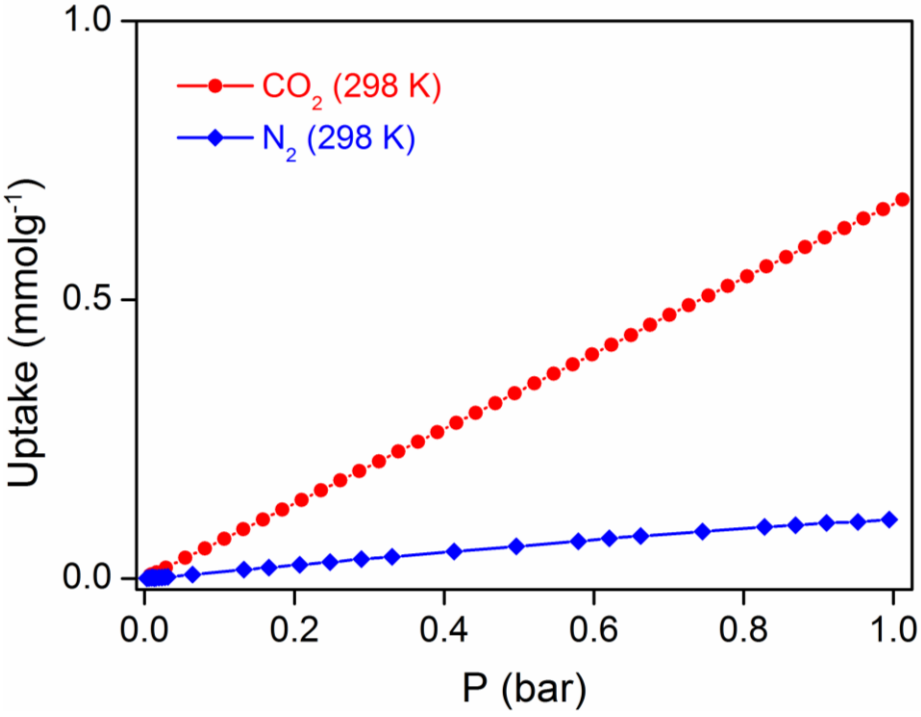

Fig. S18. CO_2 and N_2 sorption isotherms for ZIF-8.

Q_{st} Calculation - Virial Fitting for SIFSIX-18-Ni.

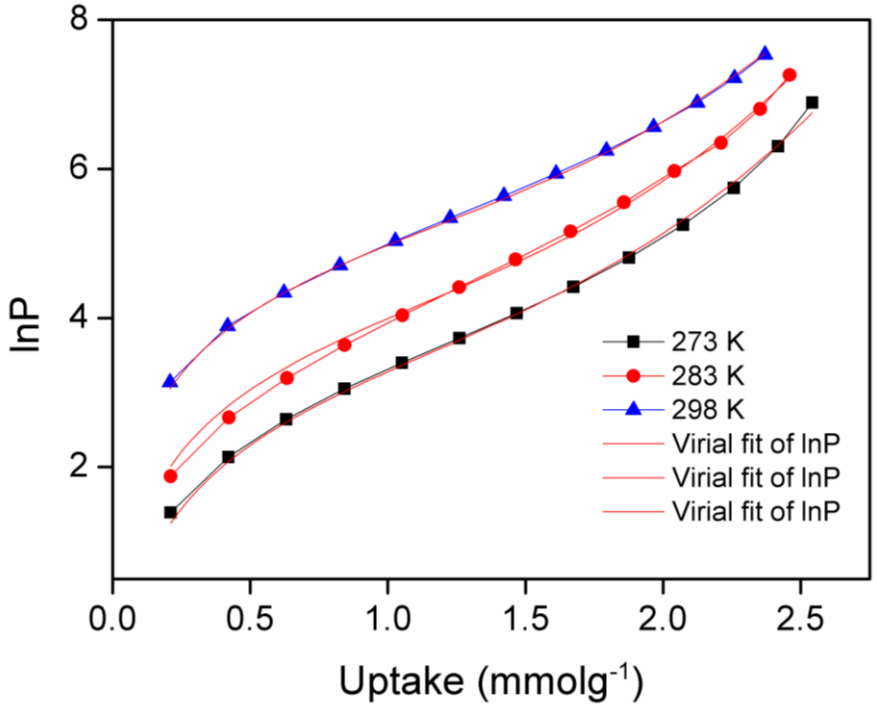

Fig. S19. Fitting of the isotherm data for SIFSIX-18-Ni-β to the virial equation.

Q_{st} Calculation - Virial Fitting for ZIF-8.

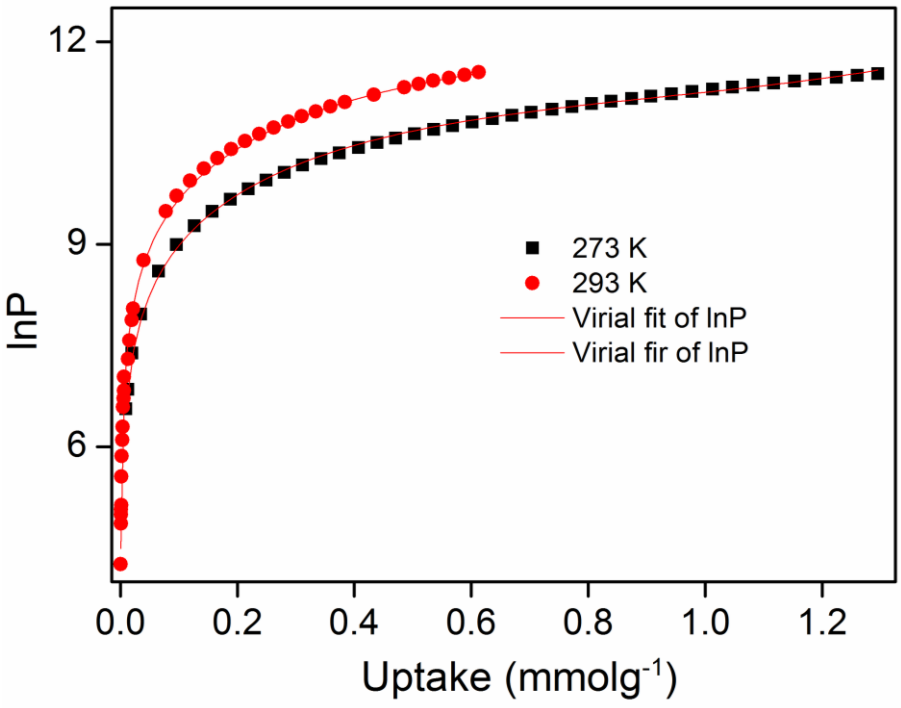

Fig. S20. Fitting of the isotherm data for ZIF-8 to the virial equation.

H_2O Sorption Isotherms.

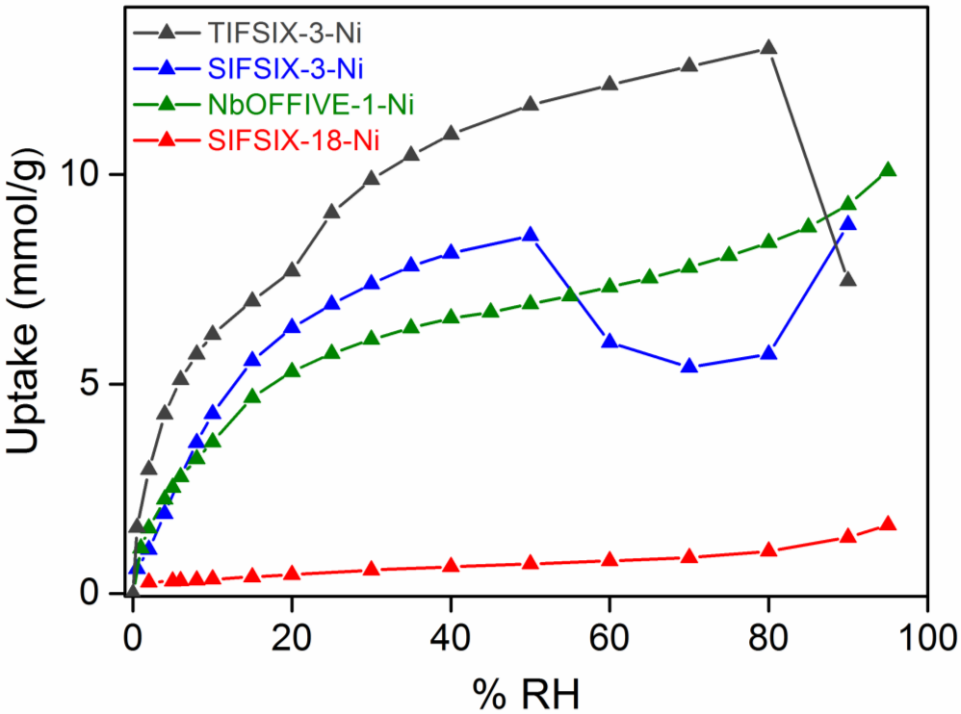

Fig. S21. H_2O sorption isotherms for SIFSIX-18-Ni-β compared with other HUMs (all recorded at 298 K).

CO_2 and H_2O Sorption Isotherms.

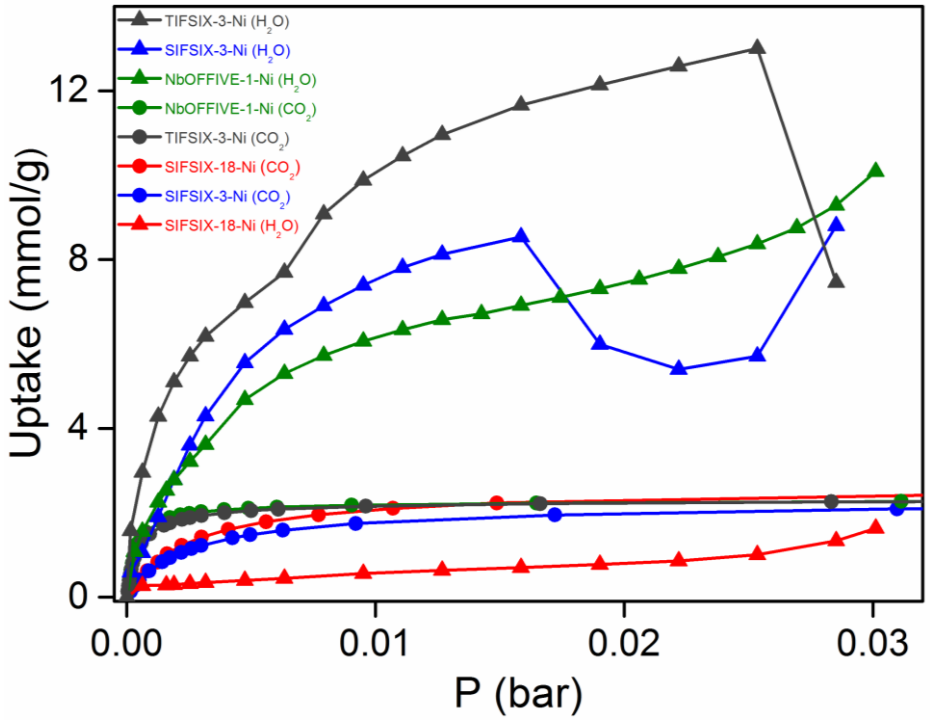

Fig. S22. Sorption isotherms (298 K) for CO_2 and H_2O for SIFSIX-18-Ni-β compared with other HUMs; pressure range until 0.03 bar i.e. saturation pressure of H_2O at 298 K.

Vacuum DVS *vs.* Intrinsic DVS H_2O sorption.

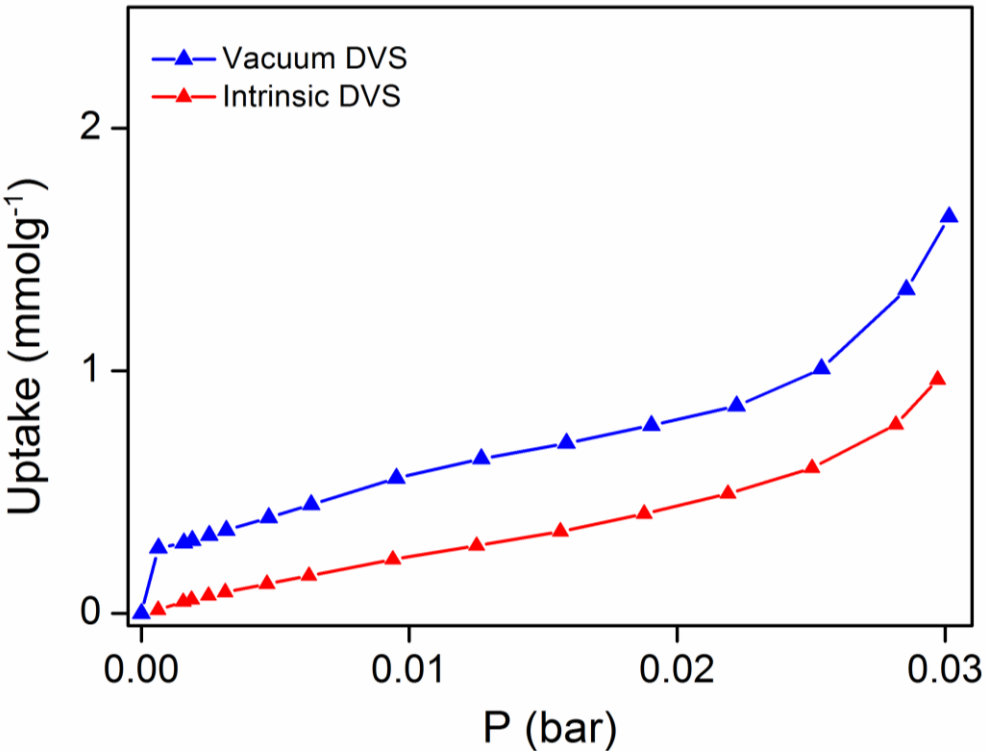

Fig. S23. H_2O sorption isotherms (298 K) of SIFSIX-18-Ni-β for vacuum DVS and intrinsic DVS experiments.

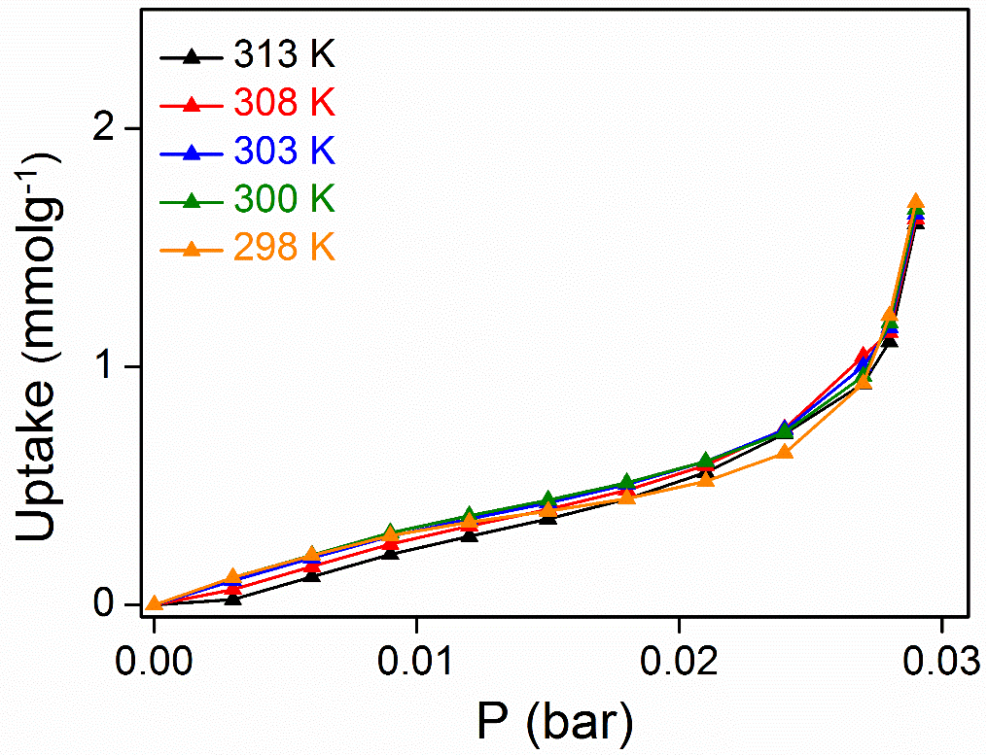

Fig. S24. H_2O sorption isotherms of SIFSIX-18-Ni-β recorded at different temperatures by intrinsic DVS experiments.

CO_2/H_2O IAST selectivities (S_{CW}).

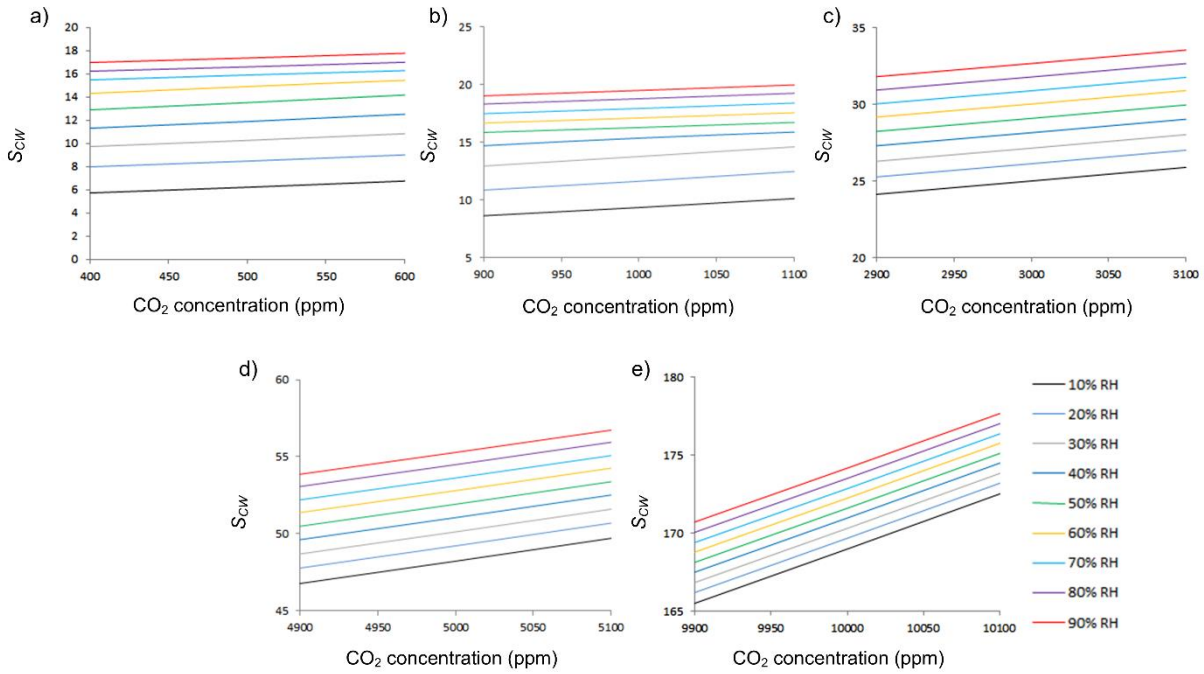

Fig. S25. Humidity-dependent CO_2/H_2O selectivities (S_{CW}) for SIFSIX-18-Ni-β at 298 K.

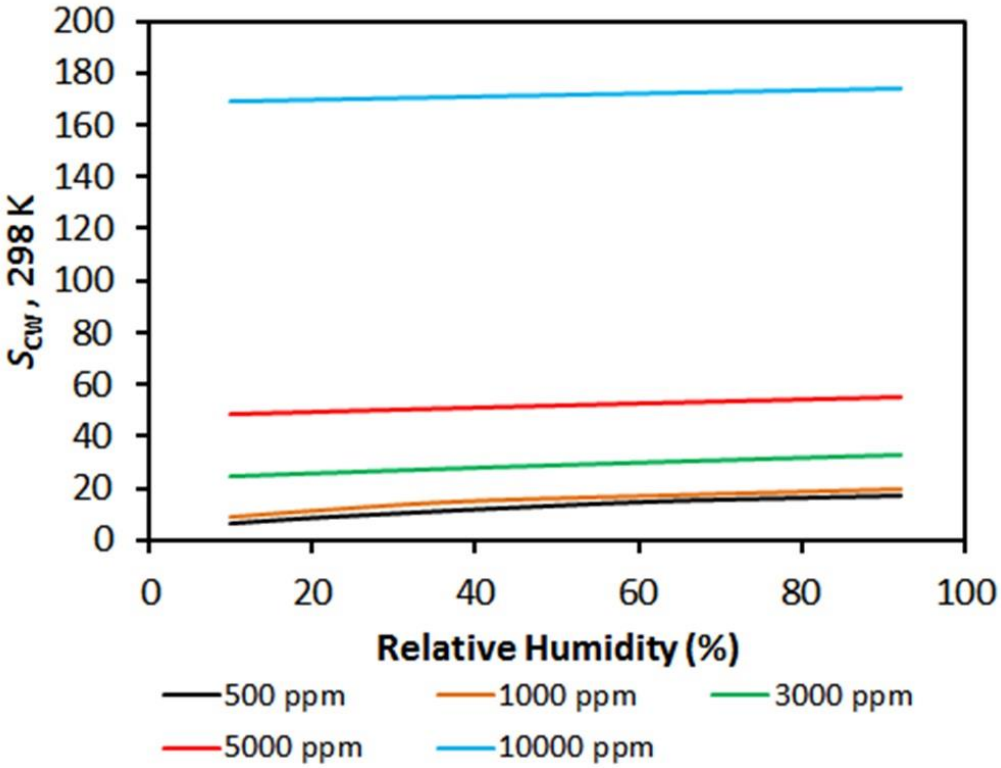

Fig. S26. CO_2/H_2O selectivities (S_{CW}) for SIFSIX-18-Ni-β under different CO_2 concentrations at 298 K.

Results from breakthrough experiments.

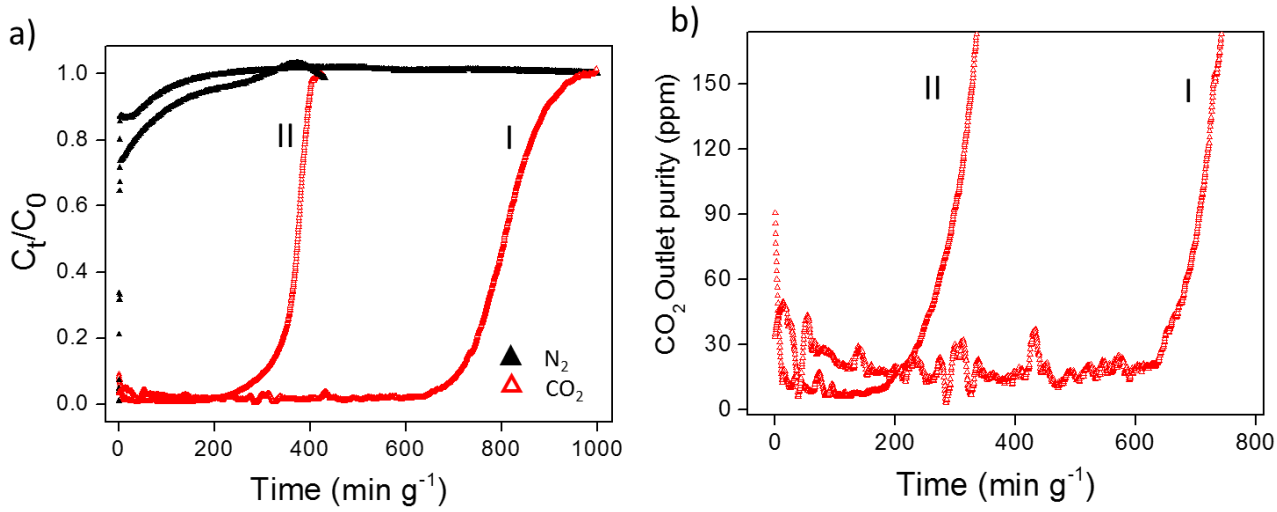

Fig. S27. 0.1/99.9 (v/v) CO_2/N_2 breakthrough profiles and CO_2 effluent purities for SIFSIX-18-Ni-β under dry and 74% RH conditions; flow rate = 20 cm^3 min^{-1}. a) 1000 ppm CO_2/N_2 (*v/v* = 0.1/99.9 %) breakthrough profiles for **SIFSIX-18-Ni-*β*** under (I) dry and (II) 74 % RH condition, **b**) CO_2 effluent purity in ppm; flow rate = 20 cm^3 min^{-1}.

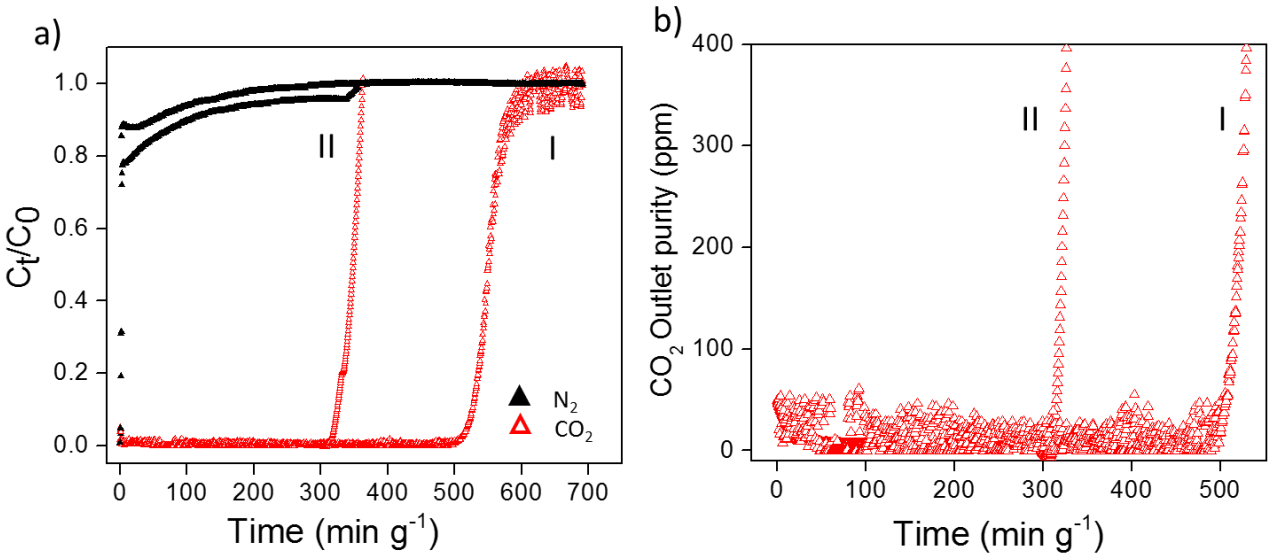

Fig. S28. 0.3/99.7 (v/v) CO_2/N_2 breakthrough profiles and CO_2 effluent purities for SIFSIX-18-Ni-β under dry and 74% RH conditions; flow rate = 20 cm^3 min^{-1}. a) 3000 ppm CO_2/N_2 (*v/v* = 0.3/99.7 %) breakthrough profiles for **SIFSIX-18-Ni-*β*** under (I) dry and (II) 74 % RH condition, **b**) CO_2 effluent purity in ppm; flow rate = 20 cm^3 min^{-1}.

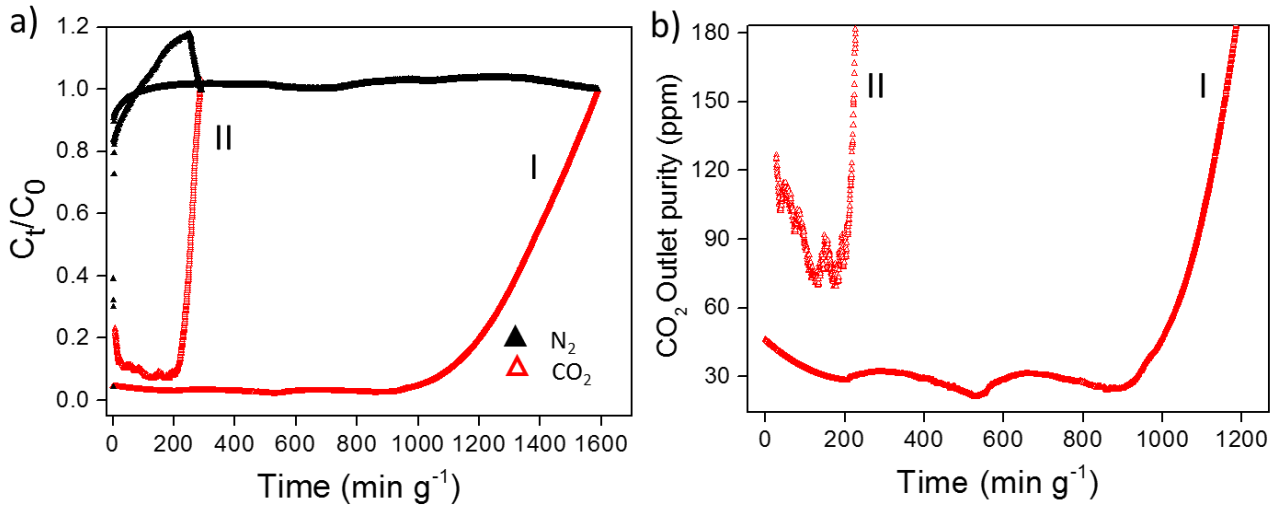

Fig. S29. 0.1/99.9 (v/v) CO_2/N_2 breakthrough profiles and CO_2 effluent purities for NbOFFIVE-1-Ni under dry and 74% RH conditions; flow rate = 20 cm^3 min^{-1}. a) 1000 ppm CO_2/N_2 (*v/v* = 0.1/99.9 %) breakthrough profiles for **NbOFFIVE-1-Ni** under (I) dry and (II) 74 % RH condition, **b**) CO_2 effluent purity in ppm; flow rate = 20 cm^3 min^{-1}.

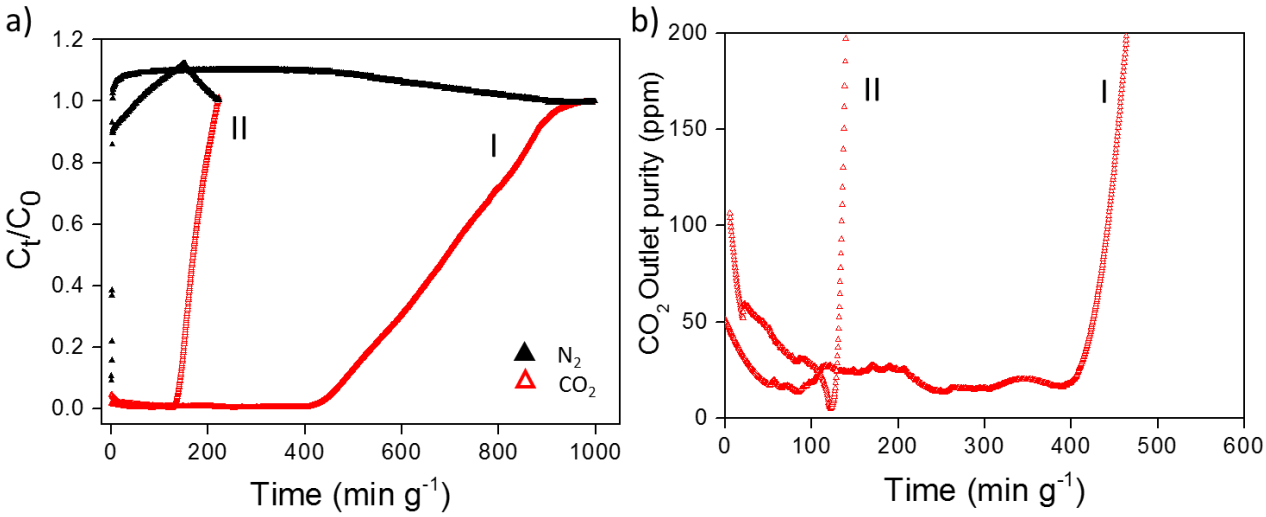

Fig. S30. 0.3/99.7 (v/v) CO_2/N_2 breakthrough profiles and CO_2 effluent purities for NbOFFIVE-1-Ni under dry and 74% RH conditions; flow rate = 20 cm^3 min^{-1}. a) 3000 ppm CO_2/N_2 (*v/v* = 0.3/99.7 %) breakthrough profiles for **NbOFFIVE-1-Ni** under (I) dry and (II) 74 % RH condition, **b**) CO_2 effluent purity in ppm; flow rate = 20 cm^3 min^{-1}.

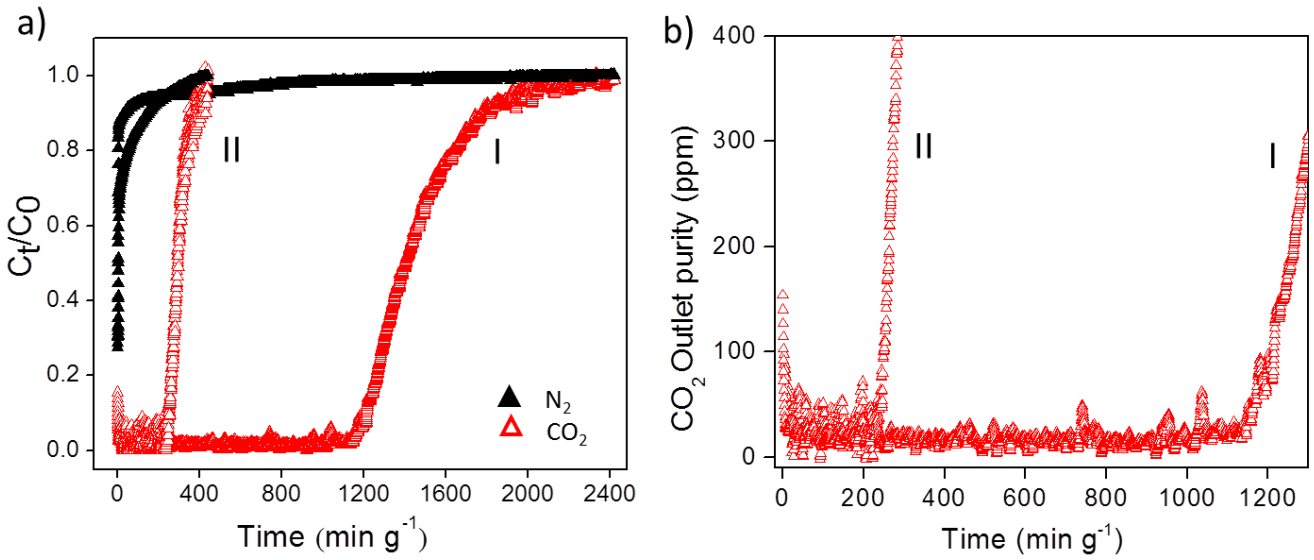

Fig. S31. 0.1/99.9 (v/v) CO_2/N_2 breakthrough profiles and CO_2 effluent purities for Zeolite 13X under dry and 74% RH conditions; flow rate = 20 cm^3 min^{-1}. a) 1000 ppm CO_2/N_2 (*v/v* = 0.1/99.9 %) breakthrough profiles for **Zeolite 13X** under (I) dry and (II) 74 % RH condition, **b**) CO_2 effluent purity in ppm; flow rate = 20 cm^3 min^{-1}.

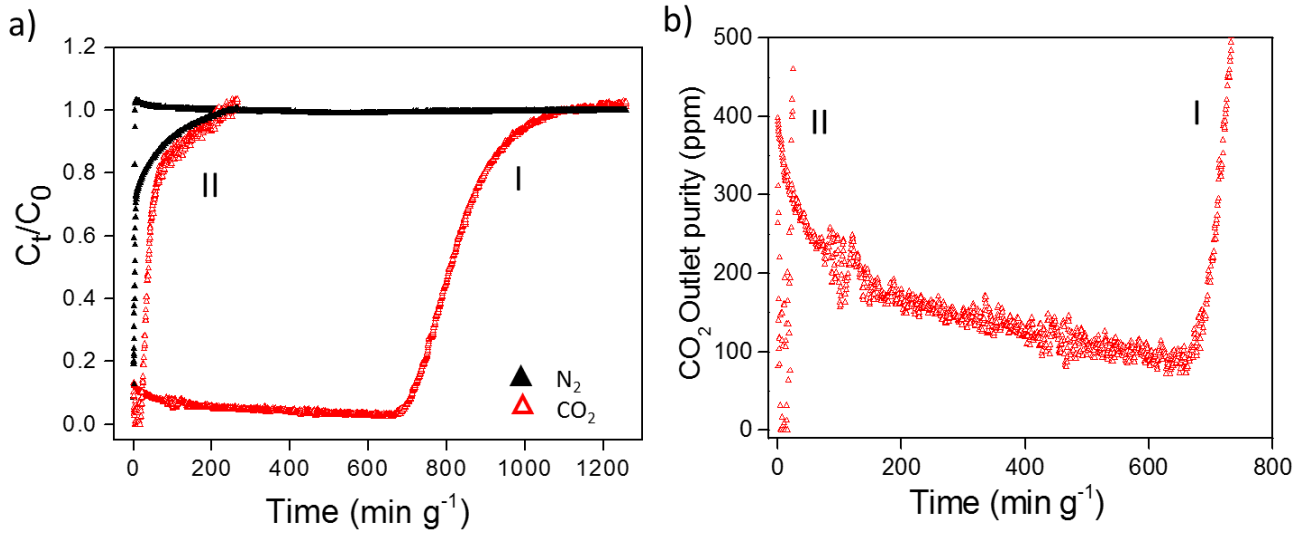

Fig. S32. 0.3/99.7 (v/v) CO_2/N_2 breakthrough profiles and CO_2 effluent purities for Zeolite 13X under dry and 74% RH conditions; flow rate = 20 cm^3 min^{-1}. a) 3000 ppm CO_2/N_2 (*v/v* = 0.3/99.7 %) breakthrough profiles for **Zeolite 13X** under (I) dry and (II) 74 % RH condition, **b**) CO_2 effluent purity in ppm; flow rate = 20 cm^3 min^{-1}.

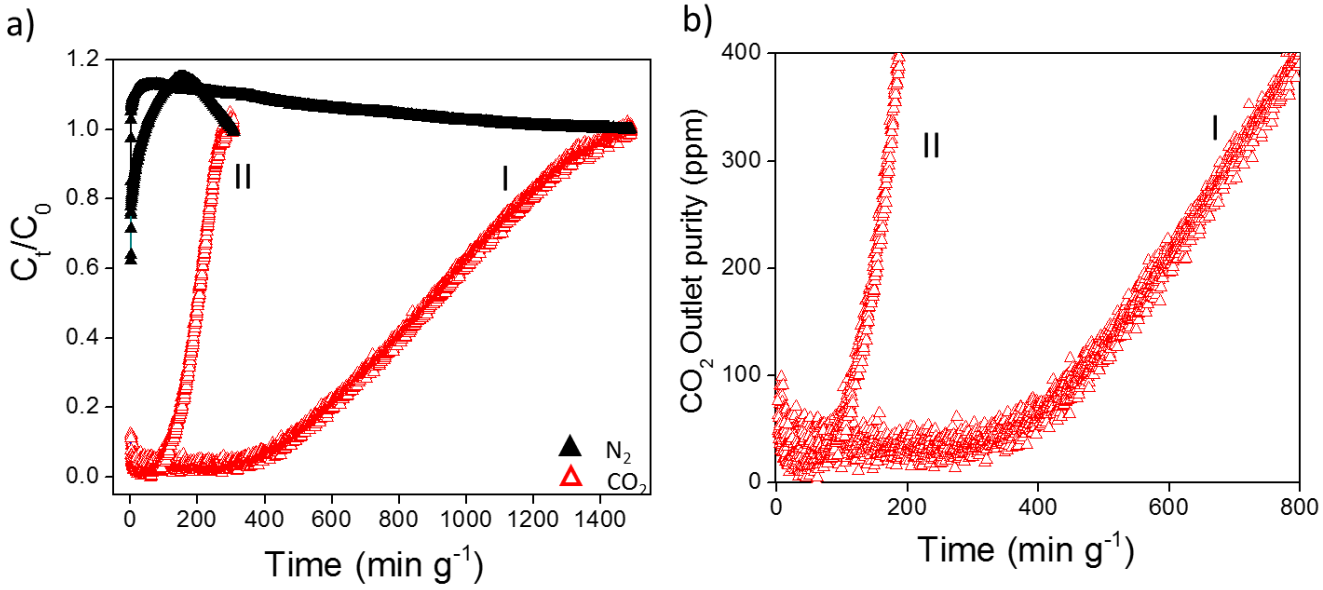

Fig. S33. 0.1/99.9 (v/v) CO_2/N_2 breakthrough profiles and CO_2 effluent purities for SIFSIX-3-Ni under dry and 74% RH conditions; flow rate = 20 cm^3 min^{-1}. a) 1000 ppm CO_2/N_2 (*v/v* = 0.1/99.9 %) breakthrough profiles for **SIFSIX-3-Ni** under (I) dry and (II) 74 % RH condition, **b**) CO_2 effluent purity in ppm; flow rate = 20 cm^3 min^{-1}.

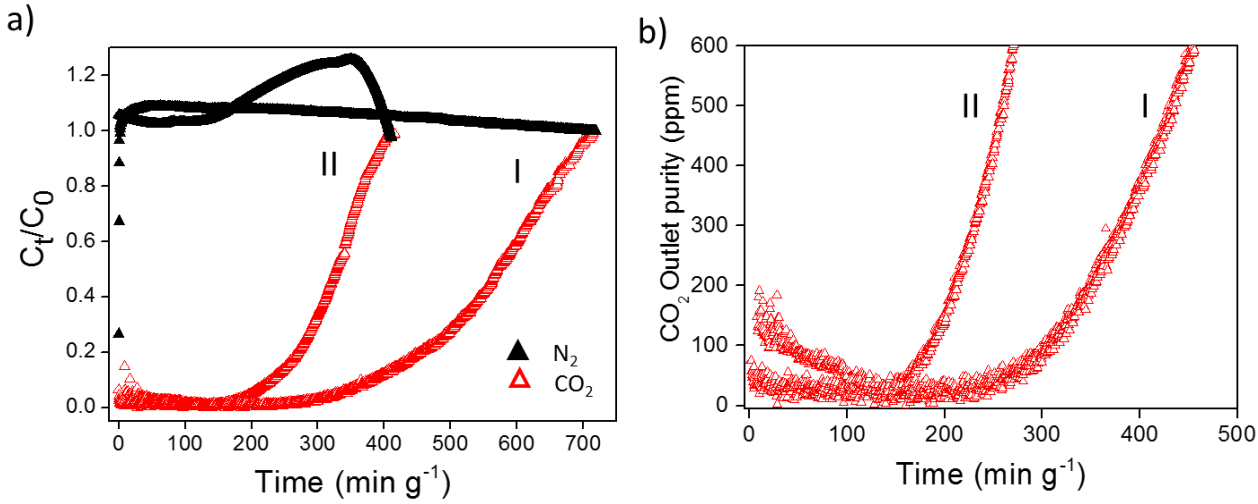

Fig. S34. 0.3/99.7 (v/v) CO_2/N_2 breakthrough profiles and CO_2 effluent purities for SIFSIX-3-Ni under dry and 74% RH conditions; flow rate = 20 cm^3 min^{-1}. a) 3000 ppm CO_2/N_2 (*v/v* = 0.3/99.7 %) breakthrough profiles for **SIFSIX-3-Ni** under (I) dry and (II) 74 % RH condition, **b**) CO_2 effluent purity in ppm; flow rate = 20 cm^3 min^{-1}.

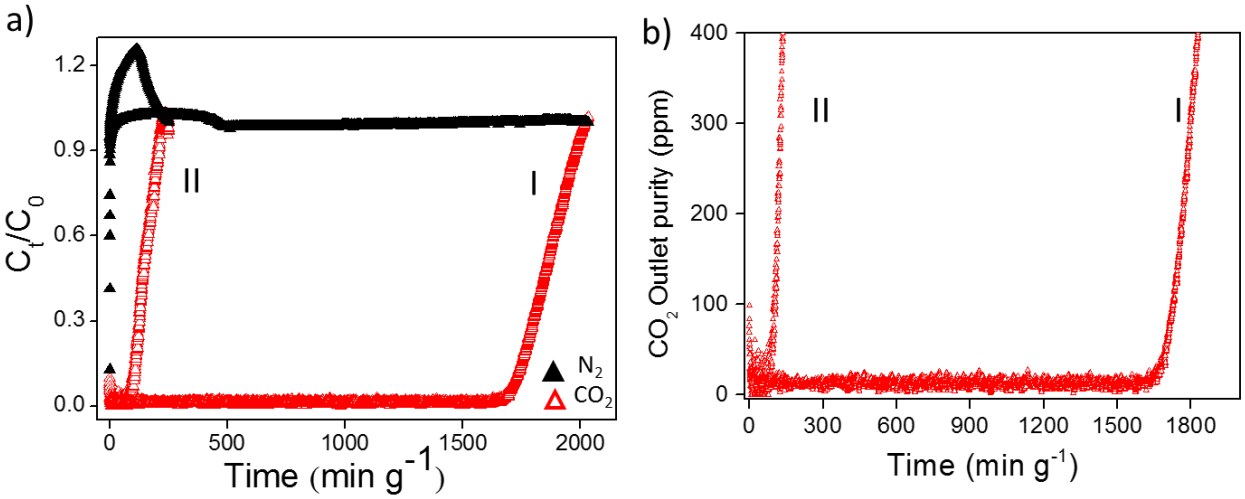

Fig. S35. 0.1/99.9 (v/v) CO_2/N_2 breakthrough profiles and CO_2 effluent purities for TIFSIX-3-Ni under dry and 74% RH conditions; flow rate = 20 cm^3 min^{-1}. a) 1000 ppm CO_2/N_2 (*v/v* = 0.1/99.9 %) breakthrough profiles for **TIFSIX-3-Ni** under (I) dry and (II) 74 % RH condition, **b**) CO_2 effluent purity in ppm; flow rate = 20 cm^3 min^{-1}.

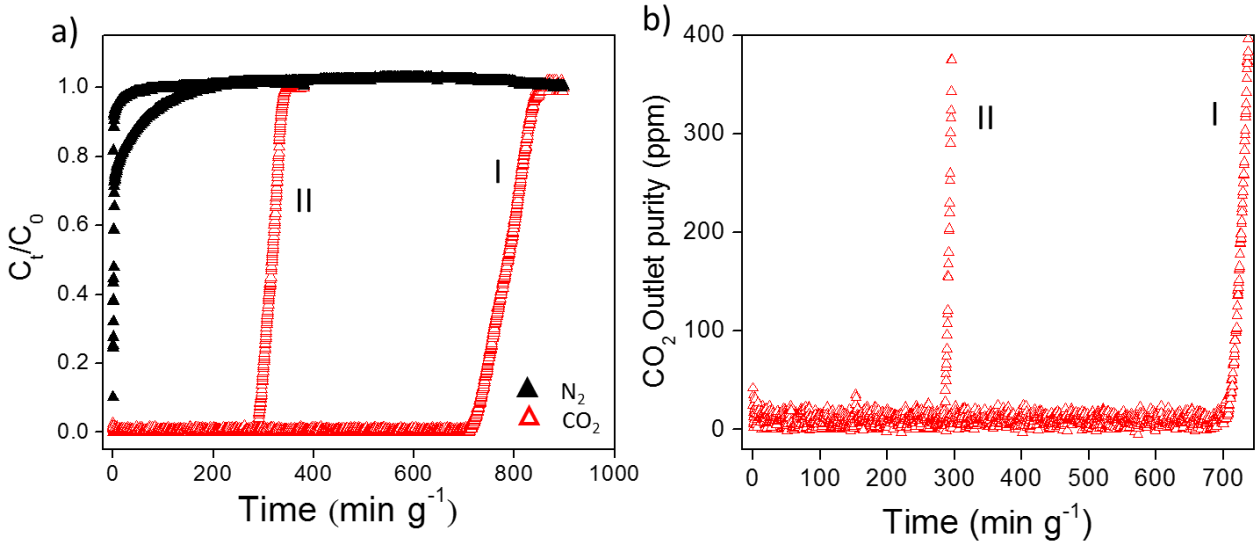

Fig. S36. 0.3/99.7 (v/v) CO_2/N_2 breakthrough profiles and CO_2 effluent purities for TIFSIX-3-Ni under dry and 74% RH conditions; flow rate = 20 cm^3 min^{-1}. a) 3000 ppm CO_2/N_2 (*v/v* = 0.3/99.7 %) breakthrough profiles for **TIFSIX-3-Ni** under (I) dry and (II) 74 % RH condition, **b**) CO_2 effluent purity in ppm; flow rate = 20 cm^3 min^{-1}.

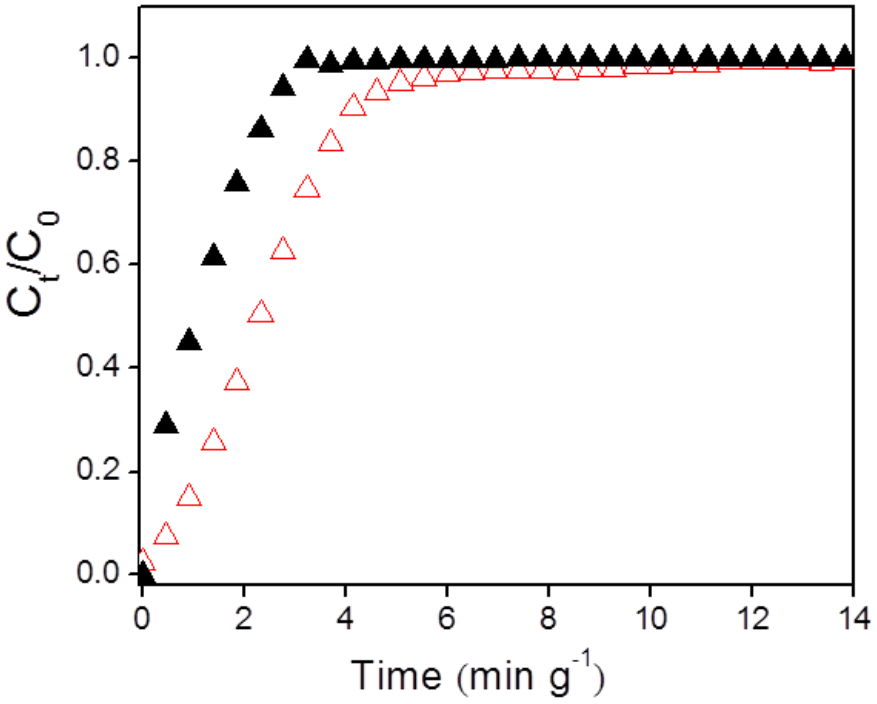

Fig. S37. 1000 ppm CO_2/N_2 (v/v = 0.1/99.9%) breakthrough profiles for ZIF-8 under dry condition, flow rate = 20 cm^3 min^{-1}.

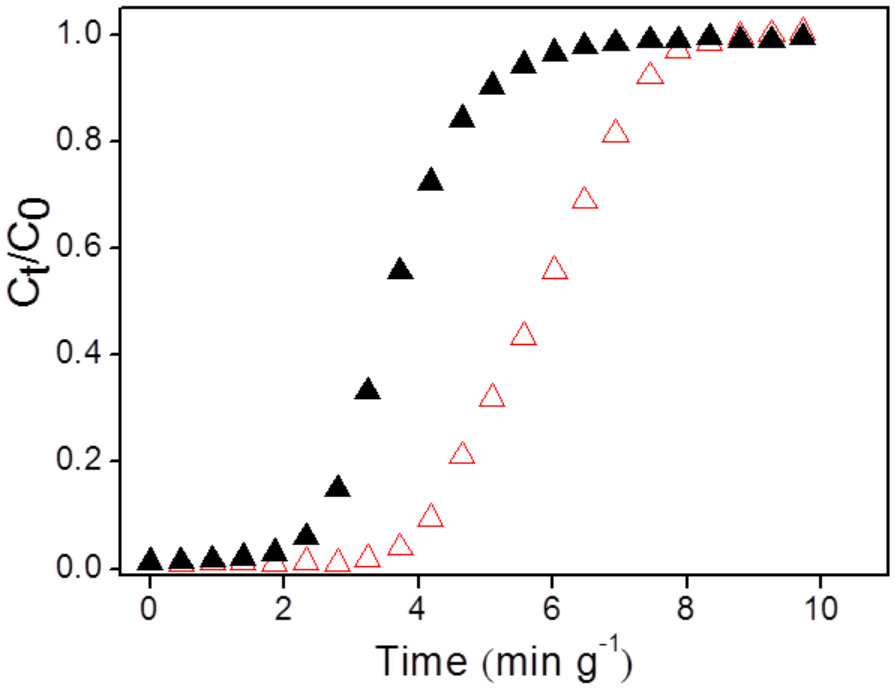

Fig. S38. 3000 ppm CO_2/N_2 (v/v = 0.3/99.7%) breakthrough profiles for ZIF-8 under dry condition, flow rate = 20 cm^3 min^{-1}.

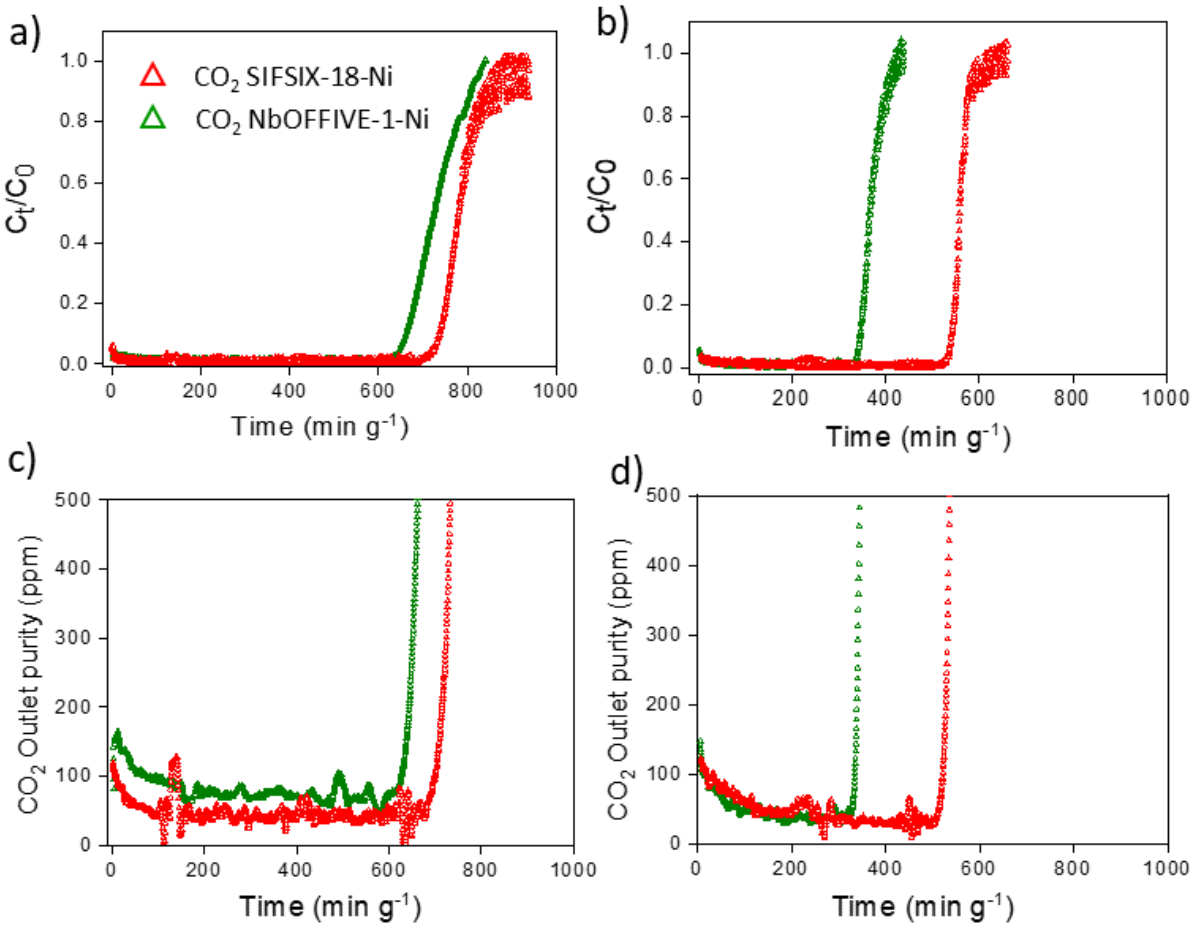

Fig. S39. 0.5/99.5 (v/v) CO_2/N_2 breakthrough profiles and CO_2 effluent purities for SIFSIX-18-Ni-β and NbOFFIVE-1-Ni under dry and 74% RH conditions; flow rate = 10 cm^3 min^{-1}. 5000 ppm CO_2/N_2 (*v/v* = 0.5/99.5 %) breakthrough profiles for **SIFSIX-18-Ni-*β*** and **NbOFFIVE-1-Ni** under (a) dry and (b) 74 % RH condition, respectively; c, d) CO_2 effluent purity in ppm under dry and 74 % RH condition, respectively; flow rate = 10 cm^3 min^{-1}.

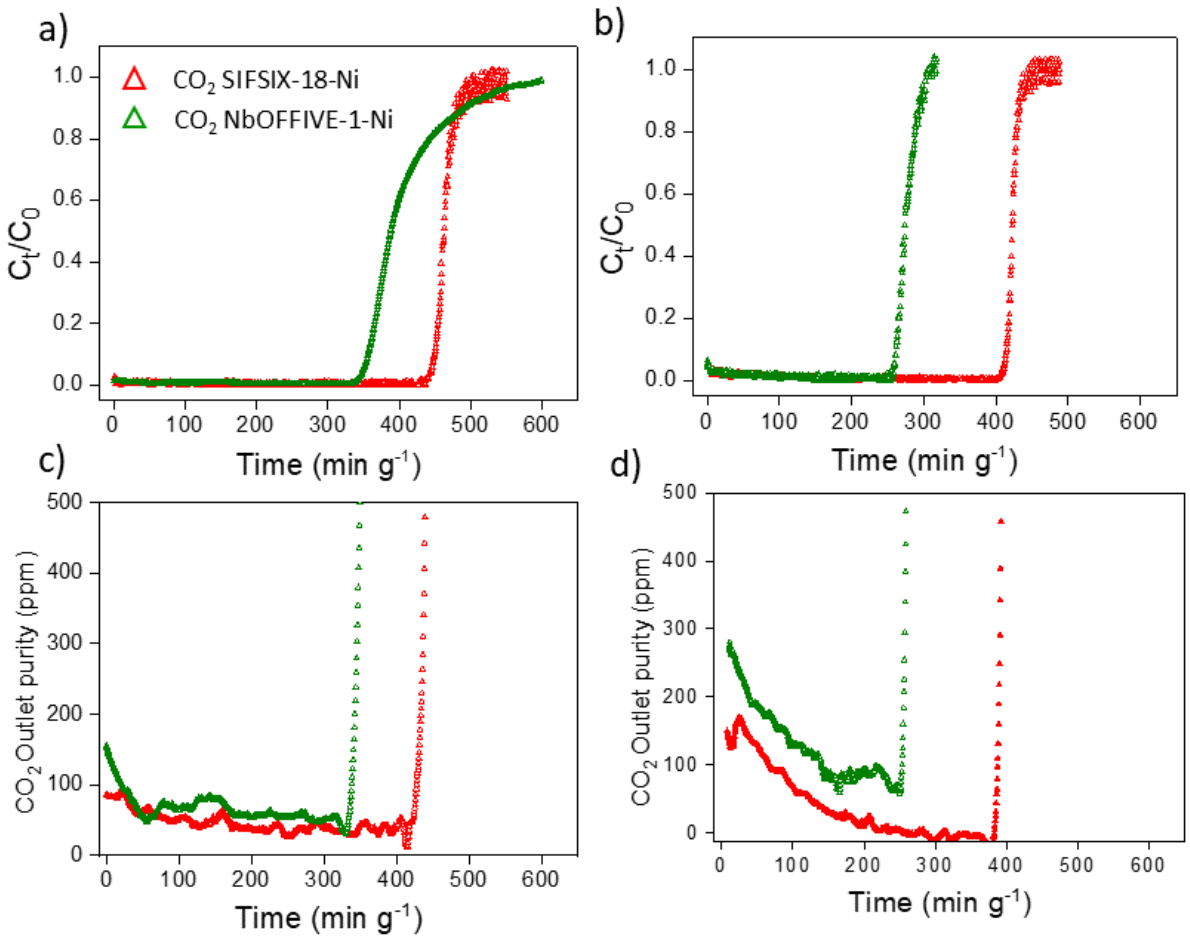

Fig. S40. 1/99 (v/v) CO_2/N_2 breakthrough profiles and CO_2 effluent purities for SIFSIX-18-Ni-β and NbOFFIVE-1-Ni under dry and 74% RH conditions; flow rate = 10 cm^3 min^{-1}. 10,000 ppm CO_2/N_2 (*v/v* = 1/99 %) breakthrough profiles for **SIFSIX-18-Ni-*β*** and **NbOFFIVE-1-Ni** under (**a**) dry and (**b**) 74 % RH condition, respectively; **c**, **d**) CO_2 effluent purity in ppm under dry and 74 % RH condition, respectively; flow rate = 10 cm^3 min^{-1}.

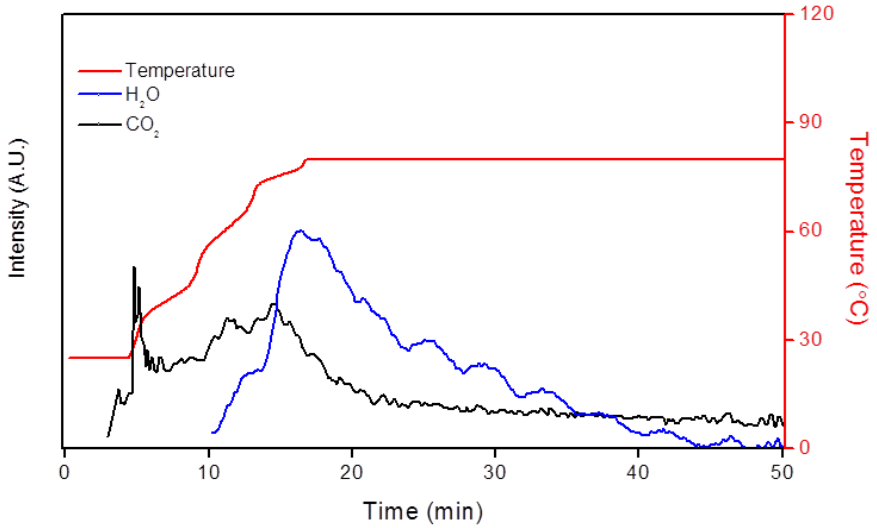

Fig. S41. Temperature-programmed desorption plot of DAC of CO_2 experiment for SIFSIX-18-Ni-β. The red curve is the temperature ramp profile used for desorption. The MS signals for CO_2 and H_2O are given by the black and blue curves, respectively.

Accelerated Stability Test.

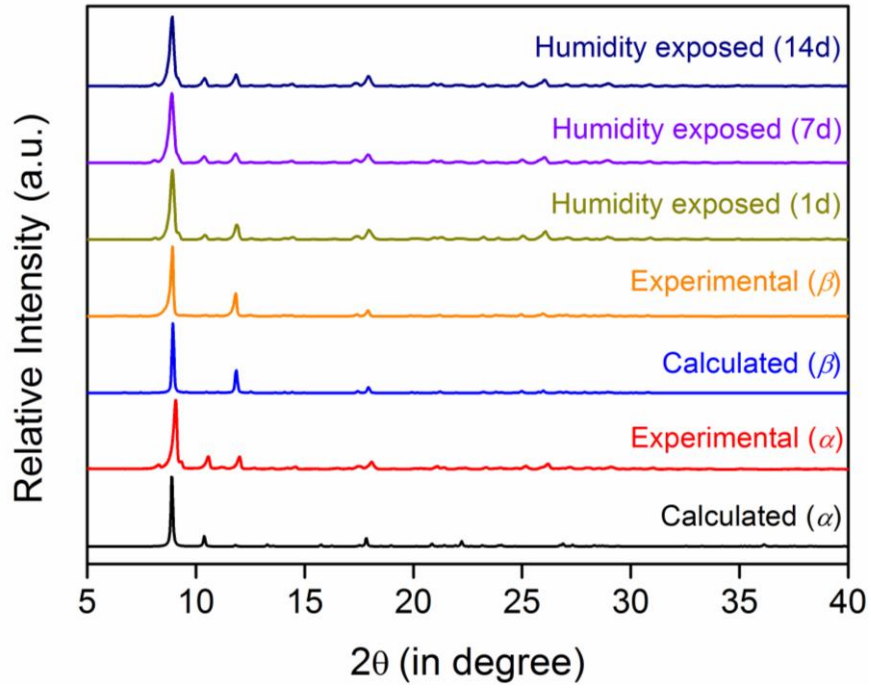

Fig. S42. PXRD profiles for SIFSIX-18-Ni before and after accelerated stability test.

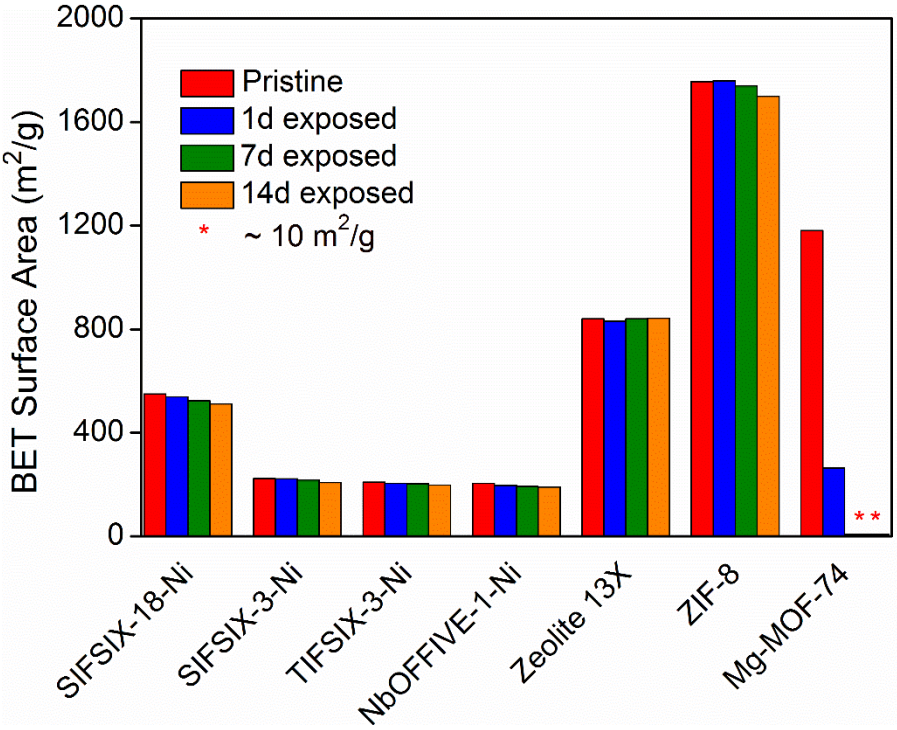

Fig. S43. BET surface areas as obtained from 77 K N_2 adsorption isotherms for SIFSIX-18-Ni and other adsorbents, after accelerated stability test.

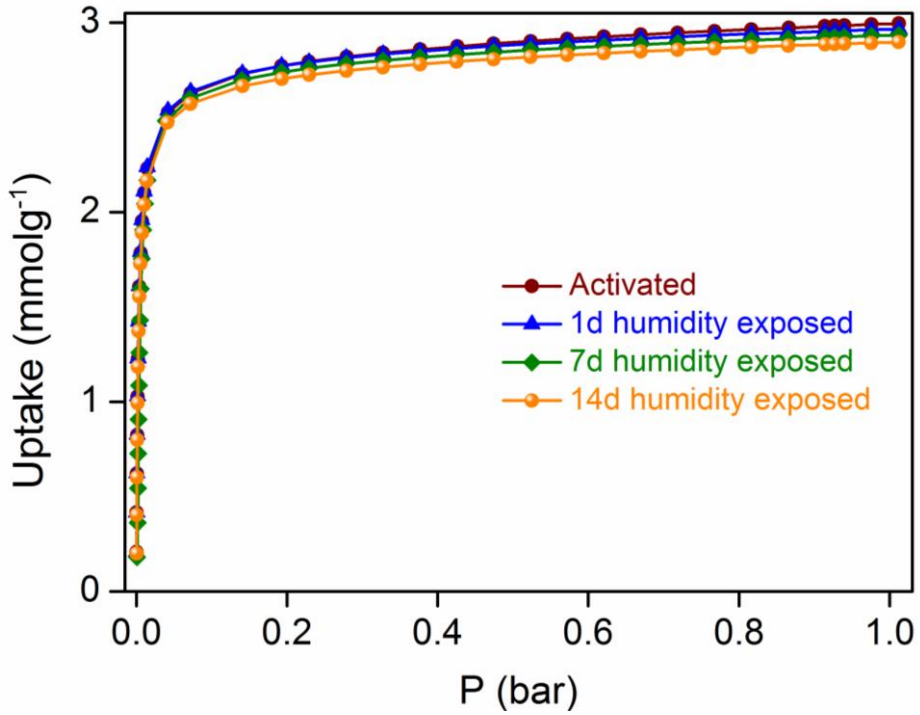

Fig. S44. CO_2 adsorption isotherms (298 K) for SIFSIX-18-Ni after accelerated stability test.

IAST derived CO_2/N_2 selectivity (S_{CN}) comparison for benchmark physisorbents.

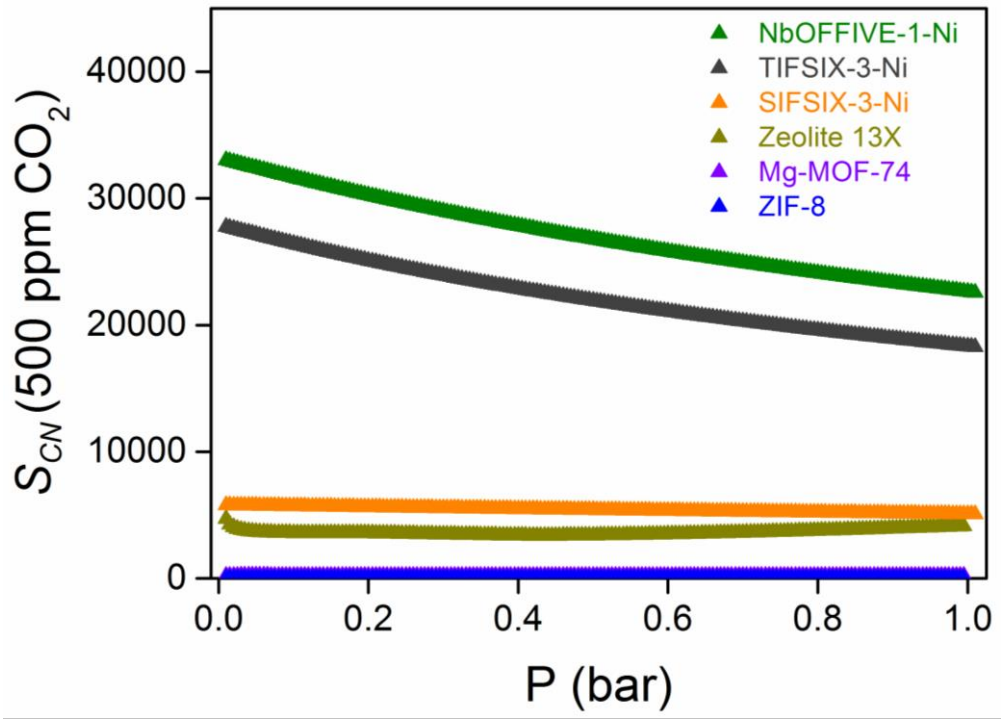

Fig. S45. IAST selectivity comparison for benchmark physisorbents at CO_2 (500 ppm): N_2 binary mixture; results for SIFSIX-18-Ni-β not included as partial sieving effect is observed.

IAST derived CO_2/O_2 selectivity (S_{CO}) for SIFSIX-18-Ni-β.

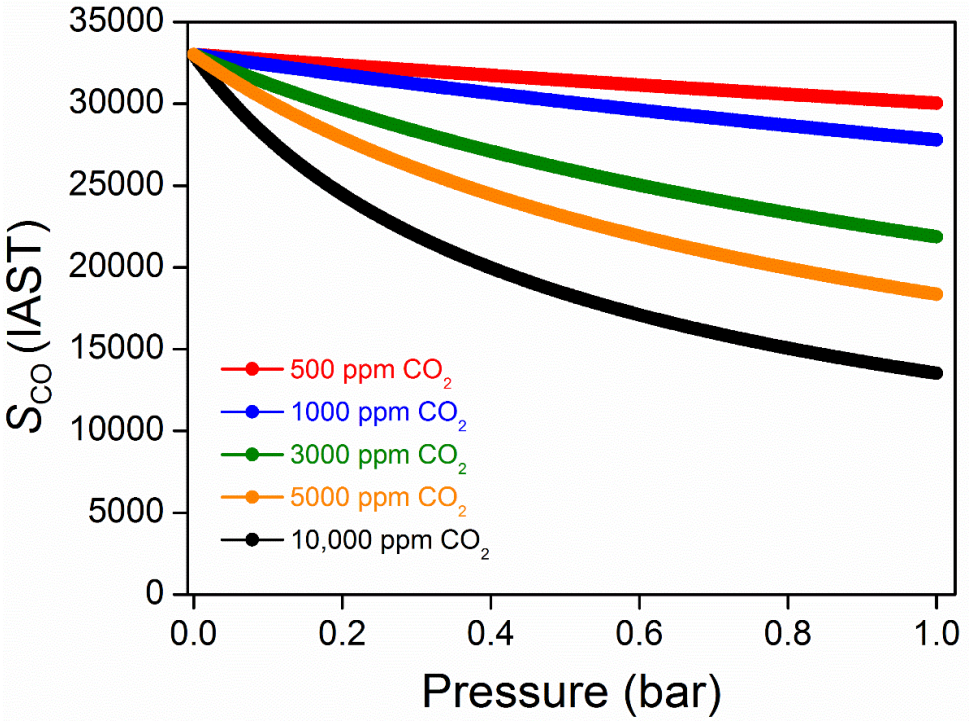

Fig. S46. IAST selectivities found in SIFSIX-18-Ni-β for CO_2/O_2 binary mixtures with varying CO_2 concentrations.

FT-IR spectra.

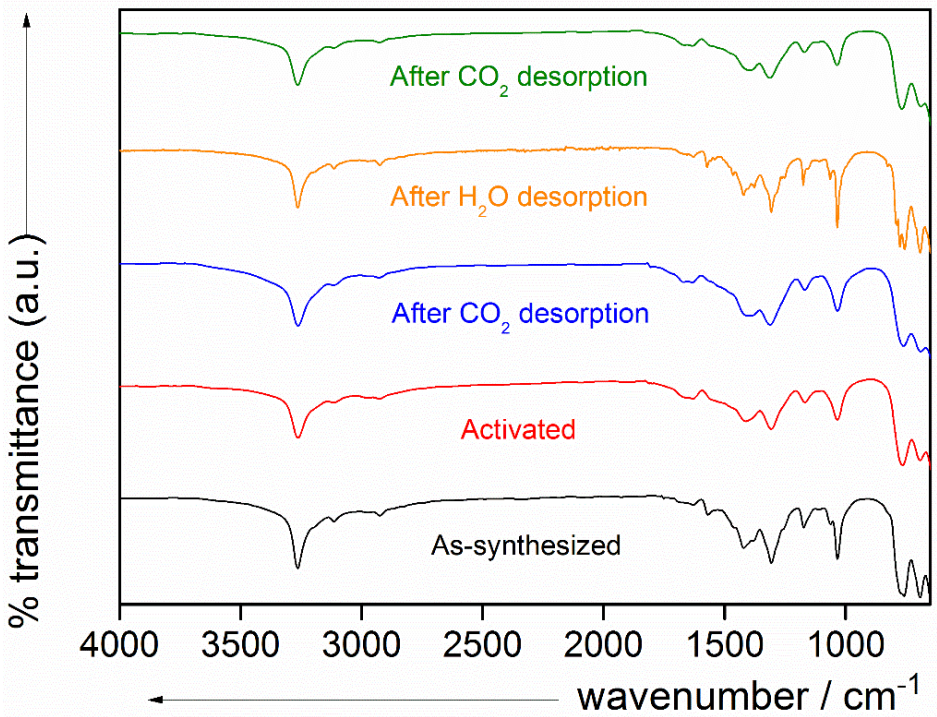

Fig. S47. FTIR spectra of SIFSIX-18-Ni: as-synthesized, activated (β), after CO_2 sorption, after H_2O sorption, and after 1-hour CO_2 dosing at 1 bar.

Gravimetric CO_2 uptake based recyclability tests (trace CO_2 mixtures: dry and wet).

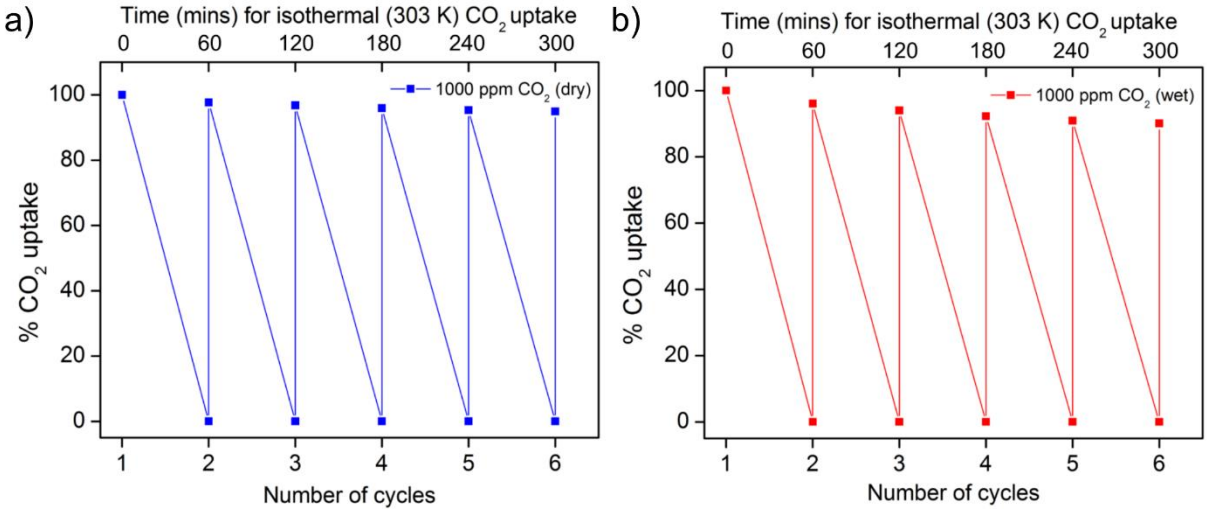

Fig. S48. 0.1/99.9 (v/v) CO_2/N_2 adsorption-desorption recyclability over 6 consecutive cycles for SIFSIX-18-Ni-β under dry and 74% RH conditions. CO_2 adsorption-desorption recyclability over 6 consecutive cycles for **SIFSIX-18-Ni-*β*** (1000 ppm CO_2/N_2 (*v/v* = 0.1/99.9 %)): a) dry, b) under 74 % RH.

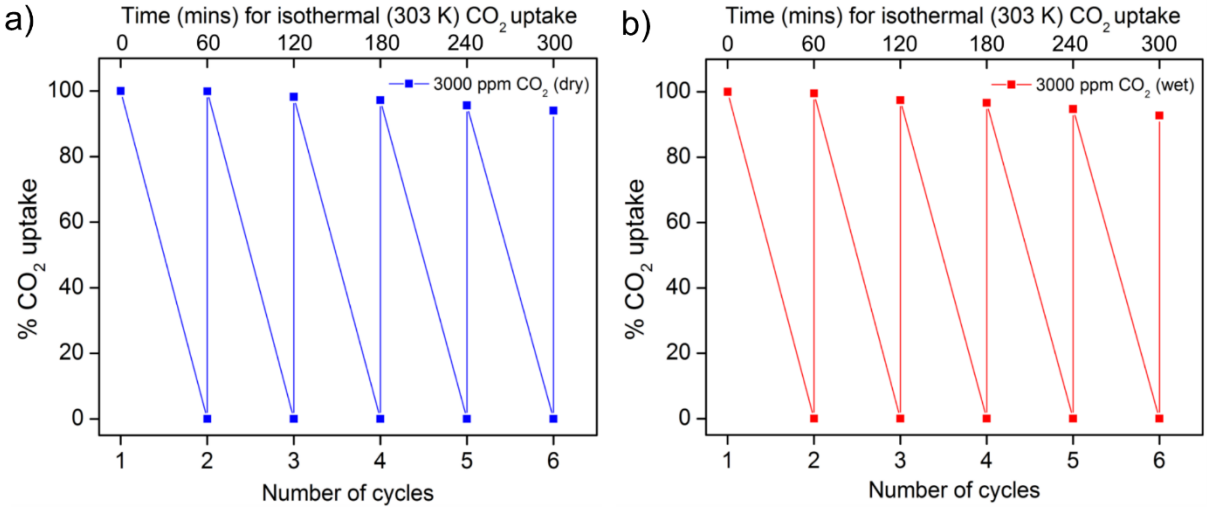

Fig. S49. 0.3/99.7 (v/v) CO_2/N_2 adsorption-desorption recyclability over 6 consecutive cycles for SIFSIX-18-Ni-β under dry and 74% RH conditions. CO_2 adsorption-desorption recyclability over 6 consecutive cycles for **SIFSIX-18-Ni-*β*** (3000 ppm CO_2/N_2 (*v/v* = 0.3/99.7 %)): a) dry, b) under 74 % RH.

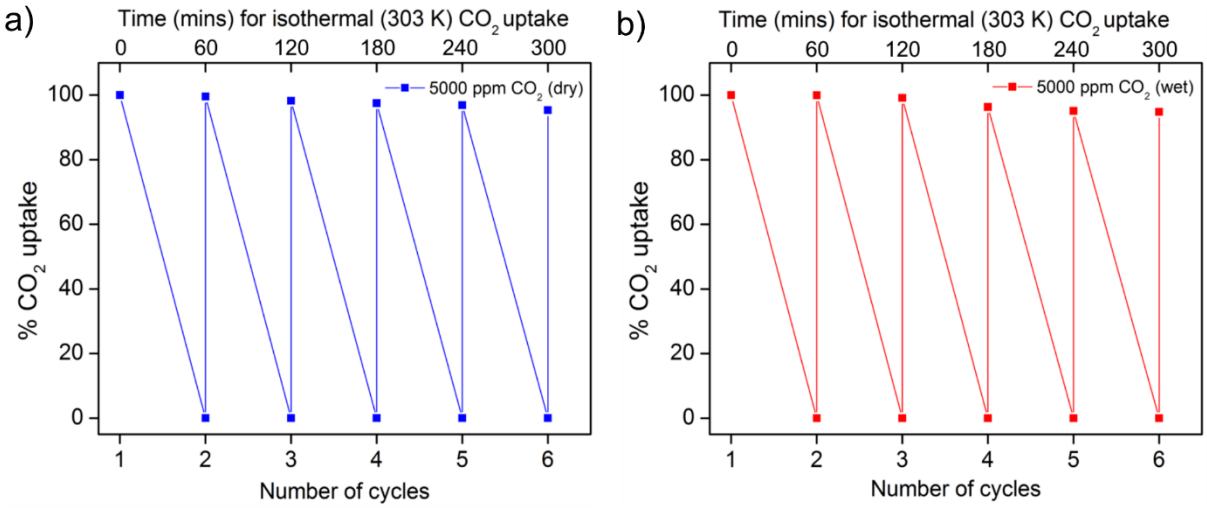

Fig. S50. 0.5/99.5 (v/v) CO_2/N_2 adsorption-desorption recyclability over 6 consecutive cycles for SIFSIX-18-Ni-β under dry and 74% RH conditions. CO_2 adsorption-desorption recyclability over 6 consecutive cycles for **SIFSIX-18-Ni-*β*** (5000 ppm CO_2/N_2 (*v/v* = 0.5/99.5 %)): a) dry, b) under 74 % RH.

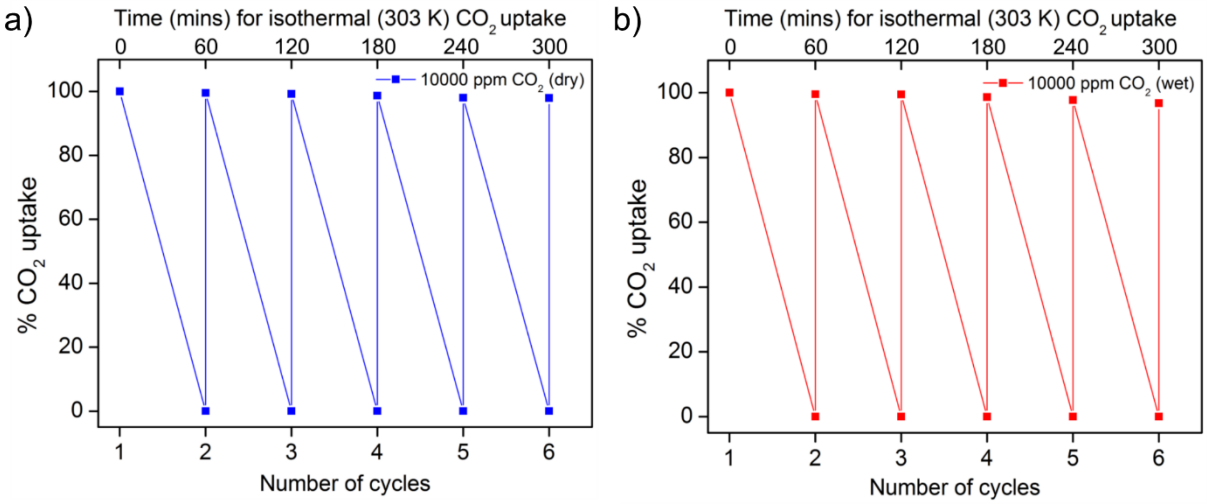

Fig. S51. 1/99 (v/v) CO_2/N_2 adsorption-desorption recyclability over 6 consecutive cycles for SIFSIX-18-Ni-β under dry and 74% RH conditions. CO_2 adsorption-desorption recyclability over 6 consecutive cycles for **SIFSIX-18-Ni-*β*** (10,000 ppm CO_2/N_2 (*v/v* = 1/99 %)): a) dry, b) under 74 % RH.

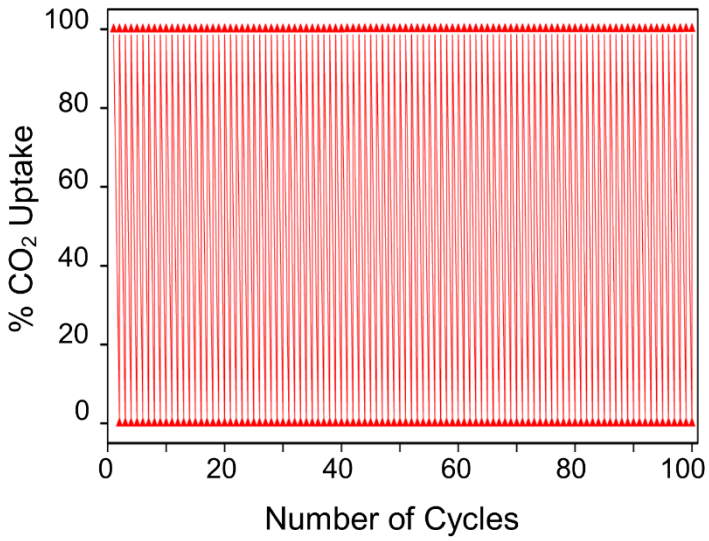

Fig. S52. CO_2 adsorption-desorption recyclability over 100 cycles for SIFSIX-18-Ni-β (1.0 bar CO_2; desorption at 348 K): for each cycle, 60 min of isothermal (303 K) gravimetric CO_2 uptake recorded on the activated sample.

Gravimetric CO_2 uptake kinetics (trace CO_2 mixtures: dry and wet).

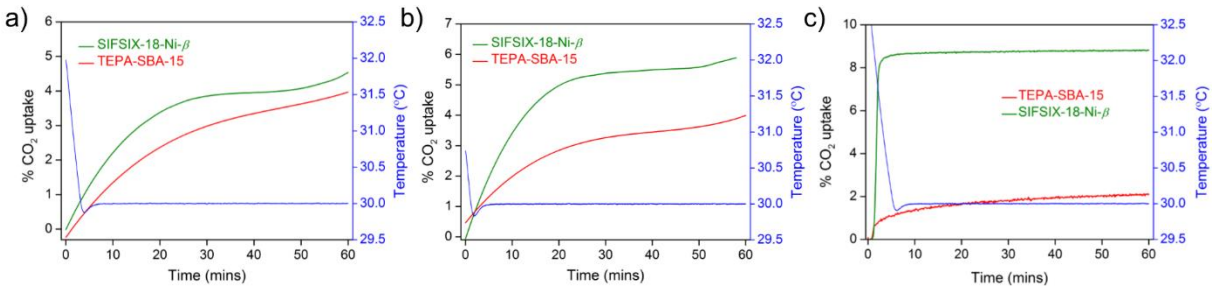

Fig. S53. Comparison of gravimetric C-capture kinetics in SIFSIX-18-Ni-β and TEPA-SBA-15 under dry conditions: a) 1000 ppm CO_2/N_2 (*v/v* = 0.1/99.9 %), b) 10,000 ppm CO_2/N_2 (*v/v* = 1/99 %) and c) 1 bar CO_2.

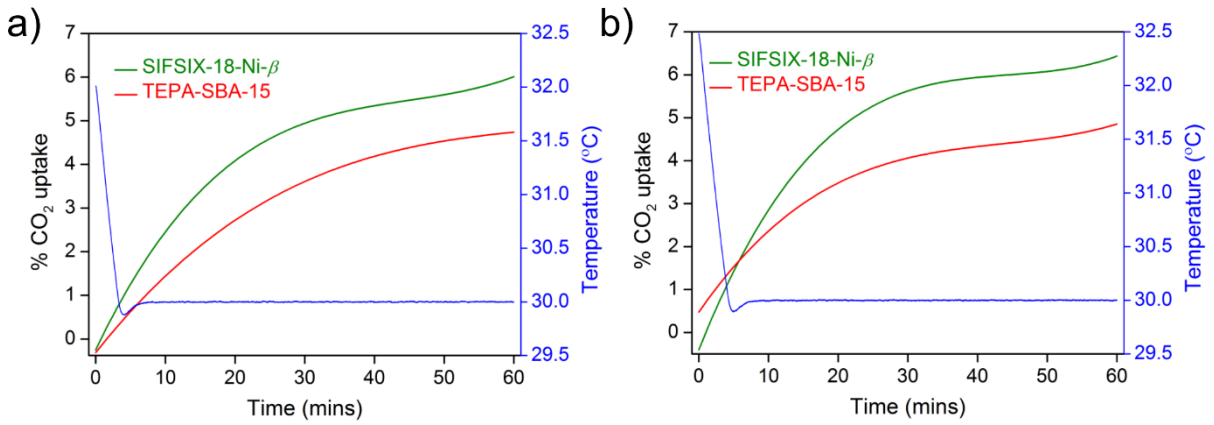

Fig. S54. Comparison of gravimetric C-capture kinetics in SIFSIX-18-Ni-β and TEPA-SBA-15 under wet conditions: a) 1000 ppm CO_2/N_2 (*v/v* = 0.1/99.9 %), b) 10,000 ppm CO_2/N_2 (*v/v* = 1/99 %), both under 74 % RH.

Structure solution.

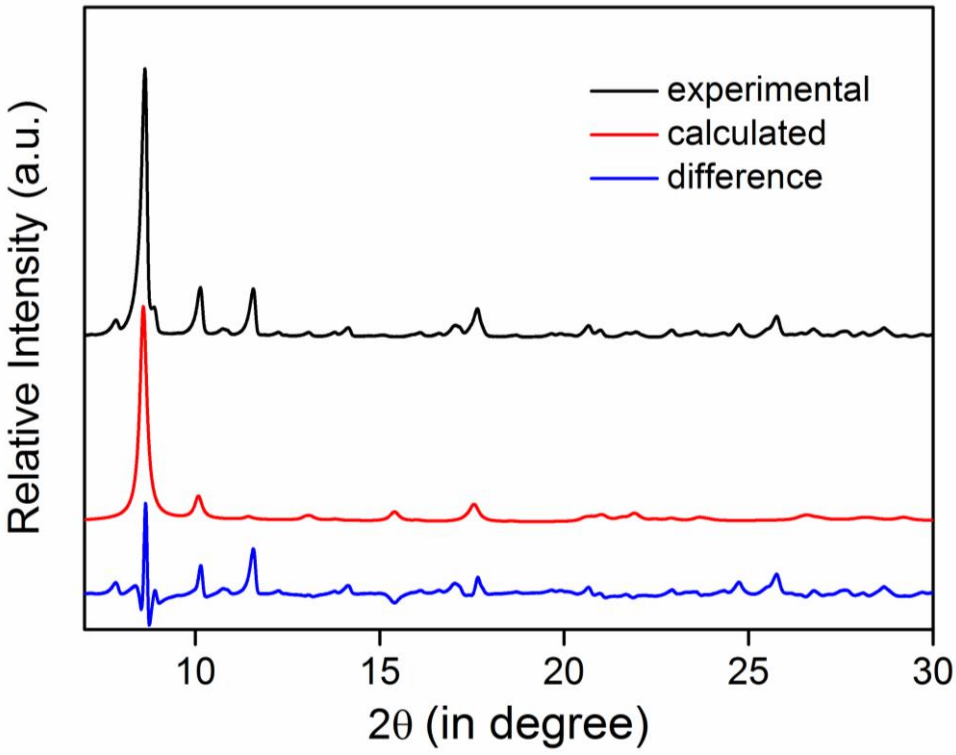

Fig. S55. Diffractograms for the Le Bail refinement of SIFSIX-18-Ni-*α*.

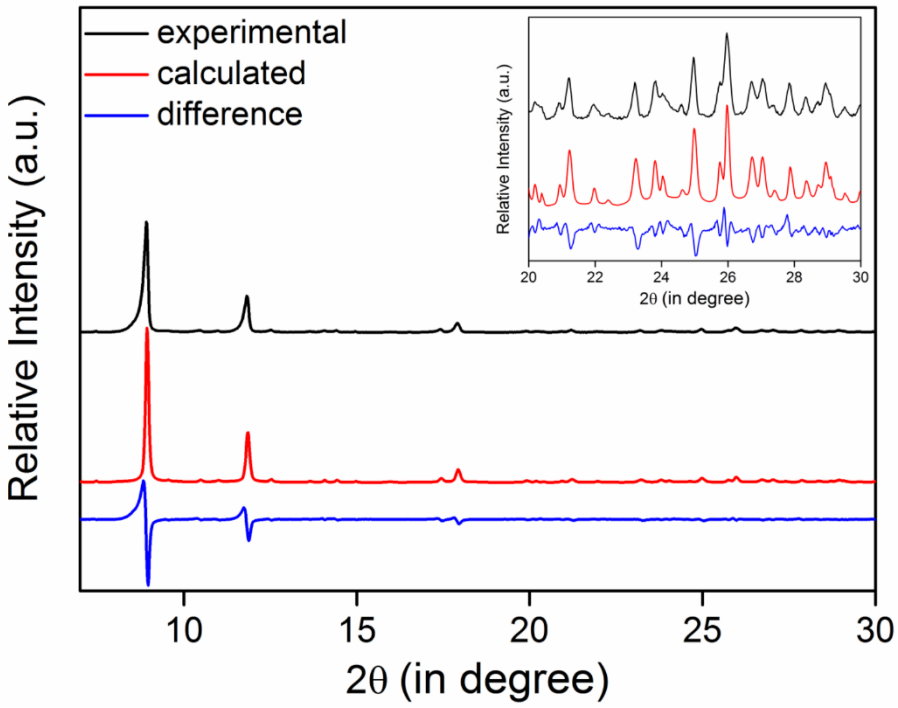

Fig. S56. Diffractograms for the Rietveld refinement of SIFSIX-18-Ni-β. Inset depicts a more detailed view of the high angle data ($20 < 2\theta < 30$).

Molecular modelling.

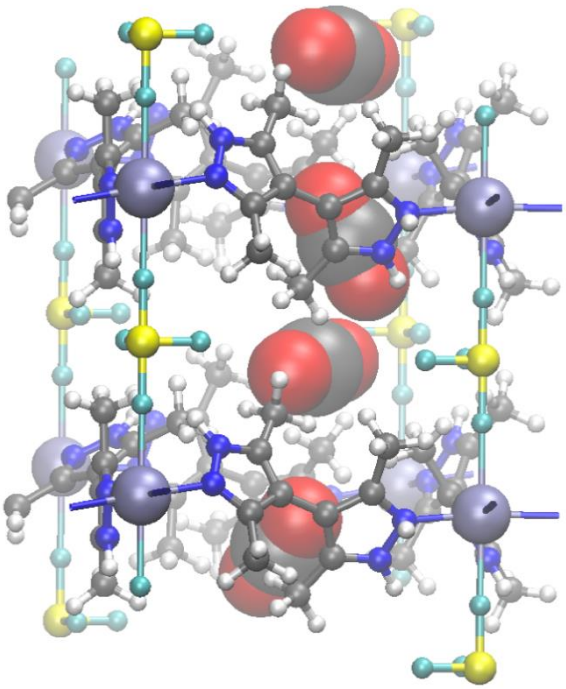

Fig. S57. Equilibrated structure of CO_2 molecules residing in the cavity of SIFSIX-18-Ni-β corresponding to a loading of 2 CO_2 per formula unit. This structure was obtained by Canonical Monte Carlo simulation at 298 K. The observed C_{CO2}...F interactions are complemented by O_{CO2}...H_{HUM} and C_{CO2}...O_{CO2} electrostatic attractions.

Schematic of gas mixing unit, gravimetric gas uptake analyser and breakthrough separation analyser.

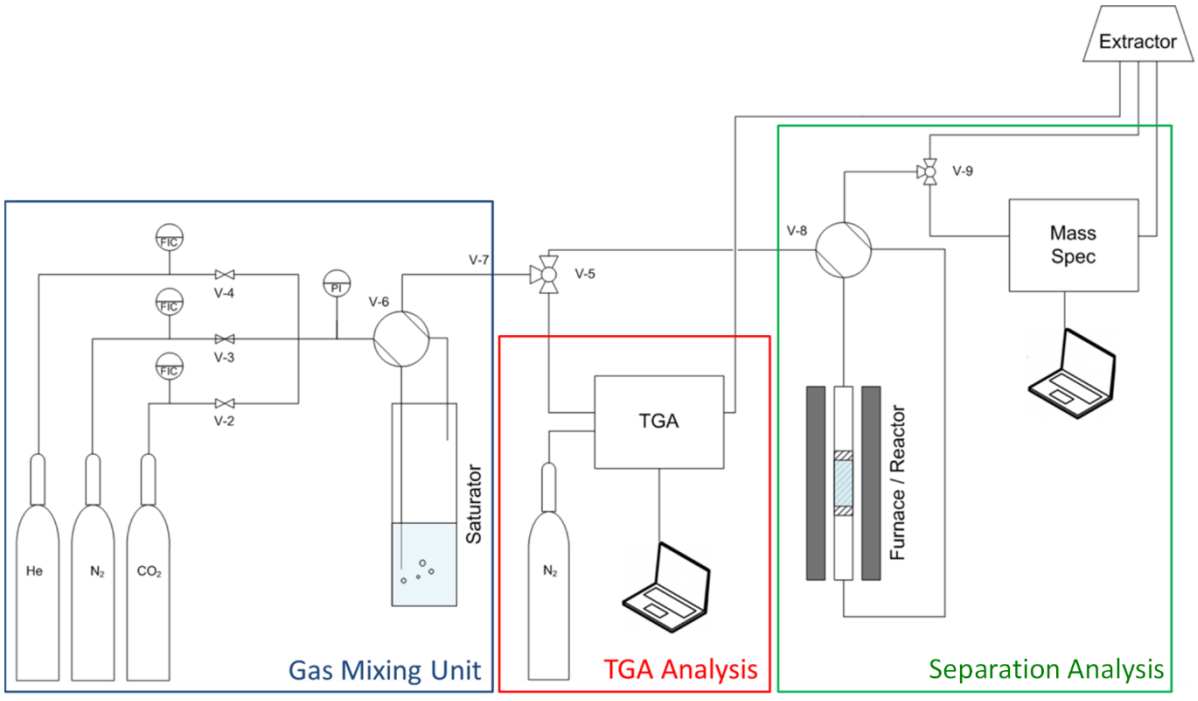

Fig. S58. Scheme of the coupled gas mixing system, TGA-based gas uptake analysis, and breakthrough separation analysis unit. The breakthrough separation analysis unit can also be used for TPD analysis.

Table S1. Calculated S_{CW} at 74% RH.

	500 ppm CO_2	5000 ppm CO_2	10,000 ppm CO_2
SIFSIX-18-Ni-β (Vacuum DVS – Ambient DVS)	16.2	54.0	173.1
SIFSIX-18-Ni-β (Vacuum DVS)	9.1	9.4	10.7
NbOFFIVE-1-Ni	0.03	0.03	0.03
ZIF-8	0.09	0.08	0.08

Table S2. Fitting parameters for SIFSIX-18-Ni-β.

Parameters	**Value**	**Standard Error**
a_0	-6400.12	210.54
a_1	569.01	142.83
a_2	-132.04	52.52
a_3	67.69	13.01
a_4	0	0
a_5	0	0
b_0	24.72	0.74
b_1	-1.20	0.48
b_2	0	0
b_3	0	0
Adj. R-Square	0.99979	

Table S3. Fitting parameters for ZIF-8.

Parameters	**Value**	**Standard Error**
a_0	-2762.63	72.77
a_1	305.70	39.45
a_2	-540.73	85.96
a_3	251.59	48.37
a_4	0	0
a_5	0	0
b_0	21.31	0.25
b_1	0	0
b_2	0	0
b_3	0	0
Adj. R-Square	0.99894	

Table S4. Dynamic breakthrough experiment details of CO_2/N_2 at 298 K and 1 bar.

Compound	Binary Gas mixture (*v/v*)	Flow rate in cm^3 min^{-1}	CO_2 uptake in cm^3 g^{-1}	CO_2 uptake in mmol g^{-1}	CO_2 Breakthrough time in min g^{-1}	CO_2/N_2 separation factor	CO_2 in outlet in ppm	% N_2 purity	%Reduction in CO_2 saturation uptake
SIFSIX-18-Ni-β	Dry 1000 ppm CO_2/N_2 [0.1/99.9 %]	20	16	0.7	715	55	18	> 99.9982	58.1
	74 % RH 1000 ppm		6.7	0.3	260	40	25	> 99.9975	
	Dry 3000 ppm CO_2/N_2 [0.3/99.7 %]		33.6	1.5	520	230	13	> 99.9987	44.6
	74 % RH 3000 ppm		18.6	0.8	316	270	10	> 99.9990	
	Dry 5000 ppm CO_2/N_2 [0.5/99.5 %]	10	38.7	1.7	735	104	48	> 99.9952	32.5
	74 % RH 5000 ppm		26.1	1.2	532	102	49	> 99.9951	
	Dry 10,000 ppm CO_2/N_2 [1/99 %]		45.6	2.0	440	217	46	> 99.9954	16.6
	74 % RH 10,000 ppm		38	1.7	410	263	38	> 99.9962	
NbOFFIVE-1-Ni	Dry 1000 ppm CO_2/N_2 [0.1/99.9 %]	20	26.7	1.2	1100	33	30	> 99.9970	82
	74 % RH 1000 ppm		4.8	0.2	220	11	90	> 99.991	
	Dry 3000 ppm CO_2/N_2 74 % RH		44	1.9	425	150	20	> 99.998	75
	74 % RH 3000 ppm		10.6	0.5	128	65	46	> 99.9954	
	Dry 5000 ppm CO_2/N_2 [0.5/99.5 %]	10	34	1.5	650	61	81	> 99.9919	55.8
	74 % RH 5000 ppm		15	0.7	333	97	51	> 99.9949	
	Dry 10,000 ppm CO_2/N_2 [1/99 %]		40	1.8	340	144	69	> 99.9931	40
	74 % RH 10,000 ppm		24	1.1	255	90	110	> 99.989	
Zeolite 13X	Dry 1000 ppm CO_2/N_2 [0.1/99.9 %]	20	27.6	1.2	1160	53	18	> 99.9982	81.5
	74 % RH 1000 ppm		5.1	0.2	240	33	30	> 99.9970	
	Dry 3000 ppm CO_2/N_2 [0.3/99.7 %]		46.8	2.1	700	19	155	> 99.9845	57.2
	74 % RH 3000 ppm		1.9	0.1	20	34	87	> 99.9913	
SIFSIX-3-Ni	Dry 1000 ppm CO_2/N_2 [0.1/99.9 %]		19.1	0.8	410	28	35	> 99.9965	79
	74 % RH 1000 ppm		4	0.2	81	31	32	> 99.9968	
	Dry 3000 ppm CO_2/N_2 [0.3/99.7 %]		35.2	1.6	322	272	11	> 99.9989	38
	74 % RH 3000 ppm		21.6	0.9	187	54	55	> 99.9945	
TIFSIX-3-Ni	Dry 1000 ppm CO_2/N_2 [0.1/99.9 %]		36.6	1.6	1670	76	13	> 99.9987	89
	74 % RH 1000 ppm		3.7	0.2	85	52	19	> 99.9981	
	Dry 3000 ppm CO_2/N_2 [0.3/99.7 %]		47.4	2.1	706	200	15	> 99.9985	62.1
	74 % RH 3000 ppm		18	0.8	283	280	10	> 99.990	
ZIF-8	Dry 1000 ppm CO_2/N_2 [0.1/99.9 %]		0.04	0.002	-	-			-
	Dry 3000 ppm CO_2/N_2 [0.3/99.7 %]		0.04	0.002	-	-			-

Table S5. Crystallographic data for SIFSIX-18-Ni.

	SIFSIX-18-Ni-*α* **(CCDC 1888094)**	**SIFSIX-18-Ni-*β***	**SIFSIX-18-Ni-*β*** **(CCDC 1888095)**
Refinement Method	Le Bail	Pawley	Rietveld
Formula	$C_{20}H_{28}N_8NiSiF_6$		
Mass	581.27		
Crystal system, space group	monoclinic, *P* 2_1	monoclinic, *C* 2	
***a* (Å)**	8.539(1)	14.197(2)	14.163(6)
***b* (Å)**	14.965(1)	13.838(2)	13.869(5)
***c* (Å)**	13.335(1)	7.4929(5)	7.493(1)
***α* (°)**	90	90	90
***β* (°)**	94.42(4)	94.60(3)	94.78(5)
***γ* (°)**	90	90	90
Volume (Å^3)	1698.91	1467.34	1466.68
***ρ* (g·cm^{-3})**	1.08	1.31	1.32
Temp (K)	293	393	
***λ* (Å)**	1.540598		
2*θ* range	$6.70 \leq 2\theta \leq 31.01$	$4.02 \leq 2\theta \leq 49.99$	
R_p	0.1288	0.0717	0.1683
wR_p	0.1812	0.1070	0.2311
R_{bragg}	-	-	0.1174
R_{exp}	0.0075	0.0157	
R(F)	-	0.0446	-
R(F^2)	-	0.0782	-
GoF	24.04	6.97	14.757
Observations	14816	2752	2705
Reflections	82	141	63